

Dust extinctions for an unbiased sample of GRB afterglows

S. Covino^{1*}, A. Melandri¹, R. Salvaterra², S. Campana¹, S. D. Vergani^{3,1},
M.G. Bernardini¹, P. D’Avanzo¹, V. D’Elia^{4,5}, D. Fugazza¹, G. Ghirlanda¹,
G. Ghisellini¹, A. Gomboc^{6,7}, Z.P. Jin^{8,1}, T. Kruehler⁹, D. Malesani⁹,
L. Nava¹⁰, B. Sbarufatti¹, and G. Tagliaferri¹

¹INAF / Brera Astronomical Observatory, via Bianchi 46, 23807, Merate (LC), Italy

²INAF / IASF Milano, via E. Bassini 15, 20133, Milano, Italy

³GEPI, Observatoire de Paris, CNRS, Univ. Paris Diderot, 5 place Jules Janssen, 92190, Meudon, France

⁴INAF / Rome Astronomical Observatory, via Frascati 33, 00040, Monteporzio Catone (Roma), Italy

⁵ASI Science Data Centre, Via Galileo Galilei, 00044, Frascati (Roma) Italy

⁶Faculty of Mathematics and Physics, University of Ljubljana, Jadranska 19, 1000 Ljubljana, Slovenia

⁷Centre of Excellence Space-si, Aškerčeva cesta 12, 1000 Ljubljana, Slovenia

⁸Purple Mountain Observatory, Chinese Academy of Sciences, Nanjing 210008, China

⁹Dark Cosmology Centre, Niels Bohr Institute, University of Copenhagen, Juliane Maries Vej 30, 2100, Copenhagen, Denmark

¹⁰APC, Univ. Paris Diderot, CNRS/IN2P3, CEA/Irfu, Obs. de Paris, Sorbonne Paris Cité, France

ABSTRACT

In this paper we compute rest-frame extinctions for the afterglows of a sample of *Swift* γ -ray bursts complete in redshift. The selection criteria of the sample are based on observational high-energy parameters of the prompt emission and therefore our sample should not be biased against dusty sight-lines. It is therefore expected that our inferences hold for the general population of γ -ray bursts. Our main result is that the optical/near-infrared extinction of γ -ray burst afterglows in our sample does not follow a single distribution. 87% of the events are absorbed by less than 2 mag, and 50% suffer from less than 0.3-0.4 mag extinction. The remaining 13% of the afterglows are highly absorbed. The true percentage of γ -ray burst afterglows showing high absorption could be even higher since a fair fraction of the events without reliable redshift measurement are probably part of this class. These events may be due to highly dusty molecular clouds/star forming regions associated with the γ -ray burst progenitor or along the afterglow line of sight, and/or to massive dusty host galaxies.

No clear evolution in the dust extinction properties is evident within the redshift range of our sample, although the largest extinctions are at $z \sim 1.5 - 2$, close to the expected peak of the star formation rate. Those events classified as dark are characterized, on average, by a higher extinction than typical events in the sample. A correlation between optical/near-infrared extinction and hydrogen-equivalent column density based on X-ray studies is shown although the observed N_{H} appears to be well in excess compared to those observed in the Local Group. Dust extinction does not seem to correlate with GRB energetics or luminosity.

Key words: gamma-rays: bursts Optical: general Optical: ISM

1 INTRODUCTION

The study of the environments of long-duration γ -ray bursts (GRBs) is a subject of growing importance for its implications on many different research areas from GRB physics to host galaxy chemical evolution. The cosmological nature of these events makes them even more interesting, allowing to

face the fundamental problem of determining how circum-burst environmental parameters vary with the age of the universe (see Gehrels et al. 2009, for a review on this field).

One possible way to obtain information about GRB environments along the line-of-sight (LOS) is to study their optical/near infrared (NIR) spectral energy distribution (SED). This allows researchers to derive information about the intrinsic spectrum in this spectral range and to study the rest-frame extinction curve, a precious source of information about dust formation (and possibly destruction) in

* E-mail: stefano.covino@brera.inaf.it

high-redshift environments (e.g. Waxman & Draine 2000; Fruchter et al. 2001; Perna & Lazzati 2002; Draine & Hao 2002; Perna et al. 2003; Stratta et al. 2004; Chen et al. 2006b; Lü et al. 2011).

One of the first attempts to derive statistical information was carried out by Schady et al. (2007) using *Swift* data and their main results are still in agreement with our present knowledge: in most cases an extinction curve typical of the Small Magellanic Cloud (SMC) environment provides a good fit to the data and only in a few cases the extinction bump at about 2175 Å, typical of the Milky Way (MW) and the Large Magellanic Cloud (LMC) environments (e.g. Pei 1992) was singled out. Schady et al. (2007) gave also support to the idea that afterglows undetected by *Swift*-UVOT¹, in several cases classifiable as “dark” bursts (see e.g. Melandri et al. 2012, and references therein for a discussion), were those with high visual extinction (Lazzati et al. 2002). Schady et al. (2010), with a larger sample of events, studied also the effect of soft X-ray absorption, which is usually quantified with the hydrogen-equivalent column density N_{H} . They found that the ratio N_{H}/A_V , with a large scatter, is significantly larger than what measured in the Magellanic Clouds or the MW.

These studies however suffered from the limited spectral response and sensitivity of *Swift*-UVOT and the high level of inhomogeneity of the available observational data for GRB afterglows (Kann et al. 2010, 2011). The situation improved in recent years thanks to the growing attitude of teams involved in GRB follow-up to share their data for a better coverage of a specific event (e.g. Covino et al. 2008; Jin et al. 2013), and in particular for the advent of advanced instruments such as GROND² equipping the 2.2 m MPI/ESO telescope at La Silla (Chile). With its simultaneous 7-band imager, from the optical to the NIR, GROND allows to obtain homogeneous and uniformly calibrated data allowing to deal with afterglow SED determination with unprecedented reliability (e.g. Greiner et al. 2011).

The search for highly extinguished GRB afterglows requires high-quality data of adequate spectral range, and indeed studies devoted to this subject (e.g. Perley et al. 2009; Krühler et al. 2011) could identify several events with moderate ($A_V \sim 1$ mag) to high ($A_V > 2$ mag) rest-frame extinction. Greiner et al. (2011), further addressing the problem of the nature of dark GRBs, confirmed that for a large fraction of them (about 3/4) extinction is responsible for the faint optical fluxes, although still about up to 1/4 of the studied events are consistent with being high-redshift GRBs, with the optical flux depressed by intergalactic neutral hydrogen absorption.

Even better results could in principle be obtained through optical/NIR spectroscopy, although the modest covered spectral range might sometimes negatively affect SED studies. Zafar et al. (2011) studied a sample of 41 GRBs mainly observed with FORS³ equipping the VLT. After modeling the SEDs from optical to X-rays by means of broken power-laws, they remarkably found that in about half of the studied events the SEDs require a break between the

two bands consistent with a synchrotron origin, as required by the so-called GRB standard model (Piran 2004). In the remaining cases (apart from one outlier) a single power-law provides a satisfactory fit. In 63% of the cases a SMC extinction curve is preferred, and the 2175 Å extinction bump is present just in 7% of their sample. About a quarter of events is finally consistent with no absorption.

Any sample so far considered is in any case likely biased toward optically bright events. Therefore it is not probably totally surprising to see such a high fraction of virtually unreddened afterglows. This has clear impact on any inference about the nature of long GRB progenitors, usually supposed to be massive stars still in their star forming regions (Schulze et al. 2011). A likely improvement of SED modeling by means of spectral data will be possible when a large sample of afterglow observations, carried out with instruments such as the ESO X-shooter⁴ (Vernet et al. 2011), capable to cover with low-to-medium resolution the whole optical/NIR range in one shot, will be available (see, e.g., D’Elia et al. 2010; Wiersema 2011).

From a different point of view, a further step toward the characterization of extinction properties of GRB LOSs should rely on statistical considerations based on a complete sample of events according to some selection criterion. To this aim we are studying in this paper the SEDs and extinction properties of a sample of 58 GRB afterglows (the BAT6 sample) described in Salvaterra et al. (2012). All 58 GRBs in our sample have been selected to have the 1-s peak photon flux $P \geq 2.6 \text{ ph s}^{-1} \text{ cm}^{-2}$ (see Salvaterra et al. 2012, for further details) as detected by *Swift*-BAT. The resulting sample has a redshift completeness level of $\sim 95\%$ ($\sim 97\%$ of the bursts have a constrained redshift). Several papers discussing various features of interest for GRB astrophysics for this sample have been delivered so far: X-ray spectra and absorbing columns are studied in Campana et al. (2012), the percentage of dark burst population is derived in Melandri et al. (2012), spectral-energy correlations are discussed in Nava et al. (2012) and Ghirlanda et al. (2012), and general prompt/afterglow brightness correlations are derived in D’Avanzo et al. (2012).

The selection criterion based on high-energy brightness of the prompt emission avoids the introduction of biases related to the optical afterglow detection and, often, for later host galaxy identification. Yet, in general, a bright prompt emission implies a bright afterglow at any wavelength, although with a large scatter (D’Avanzo et al. 2012). Therefore in a large fraction of cases the optical data available are adequate for the analysis. The very high level of redshift completeness makes it possible for the first time to obtain representative statistics of the extinction properties of GRB LOSs from nearby ($z \sim 0.1$) to far cosmological events ($z \sim 5.5$).

In Sect. 2 we discuss the methodologies applied to the analysis of the events in our sample. In Sect. 3 we report about our main results and in Sect. 4 general conclusions are drawn. Details about the analysis for each event are discussed in Appendix A.

¹ <http://www.swift.psu.edu/uvot>

² <http://www.mpe.mpg.de/~jcg/GROND/>

³ <http://www.eso.org/sci/facilities/paranal/instruments/fors/>

⁴ <http://www.eso.org/sci/facilities/paranal/instruments/xshooter/>

2 DATA AND METHODOLOGY

In order to compute the SED for as many events as possible included in our sample, we collected all the available data including those published only in GCN⁵ short communications. In a few cases, we had access to still unpublished data or derived a new calibration (see Appendix A).

The SED in the optical/NIR range is modeled as a power-law reddened by rest-frame extinction, $f_\nu \propto \nu^{-\beta} e^{-\tau(\nu(1+z))}$, where ν is the observed frequency, z is the source redshift, $\tau(\nu)$ is the computed optical depth and β is the spectral index. We applied three possible extinction curves, namely those typical for the MW, LMC and SMC, as modeled by Pei (1992). MW extinction in our Galaxy is also considered (Schlegel et al. 1998). We did not try a more complex modeling of the extinction curve (see, e.g. Calzetti et al. 1994; Maiolino et al. 2004; Gallerani et al. 2010; Liang & Li 2010) since the inhomogeneity of the available data could easily introduce spurious results not justifying the increase in complexity in our statistical analysis. In addition, a reliable analysis of a grey extinction curves would be possible only for those events with optical/NIR and soft X-rays lying on the same spectral segment, due to the degeneracy between optical/NIR spectral normalization and the break frequency location between these two spectral regions. This would have limited the sample size of our analysis to just a small fraction of the available events. Temporal decays are modeled as power-laws, $f(t) \propto (t - t_0)^{-\alpha}$, where $t - t_0$ is the time after the burst and α the temporal index. In order not to artificially neglect the possible covariance between the spectral index and temporal decay when data are poorly sampled, temporal and spectral data are simultaneously fit. χ^2 minimization is performed by using the downhill (Nelder-Mead) simplex algorithm as coded in the `python`⁶ `scipy.optimize`⁷ library, v.0.10.0. Error search is carried out following Cash (1976) with β and E_{B-V} as parameters of interest. Throughout this paper the reported uncertainties are at 1σ level with the exception of hydrogen-equivalent column densities and X-ray spectral slopes, which are shown with 90% errors. Upper limits are at 95% confidence level. Lower limits have been derived by making use of the usually poor information available in the literature, as for instance rough upper limits published in GCNs. So, for lower limits, it is not possible to give a confidence level. They are anyway derived assuming the less demanding, in terms of required optical extinction, extrapolation of X-ray spectra to the optical band, i.e. introducing a spectral break just below the *Swift*-XRT range.

Our goal is to derive a reliable SED and extinction evaluation, therefore we did not try to model the whole light-curve of the analyzed events. We instead considered only the time interval required to firmly constrain the temporal index around the epoch when the most reliable photometric information is available. In several cases, not optimal calibration and/or inhomogeneity in the available data required to add a systematic calibration error in quadrature. We considered acceptable a fit if its null probability is better than 10%. The spectral slope was derived both considering only opti-

cal/NIR data and adding a statical prior from the analysis of roughly simultaneous X-ray data. This is an alternative procedure compared to the simultaneous fit of X-ray and optical data, since in this latter case the solution is usually dominated by the much more numerous X-ray points, making fit results less sensitive to the information provided by the optical/NIR data. We imposed that $\beta_o = \beta_x - 0.5$ or $\beta_o = \beta_x$ including the 90% error on the X-ray spectral slope. This is essentially equivalent to assume that the afterglow emission is due to synchrotron radiation and the cooling frequency is either outside or in between the X-ray and optical/NIR ranges (see, e.g., Sari et al. 1998; Zhang & Mészáros 2004, and references therein). However, this choice does not imply that the afterglow evolution can be modeled in the framework of the cosmological fireball model (see also Uhm & Zhang 2013). Results for all extinction recipes are reported in Table A10 (available only in electronic format) and details about each event fit and data selection are reported in Appendix A. In case more solutions are statistically acceptable we always chose the one obtained assuming a SMC extinction curve, for an easier comparison with most of the previous studies of GRB afterglow optical/NIR SEDs. Multiple acceptable solutions are typically possible only in case of low total extinction, when results based on different extinction recipes tend to be comparable.

For the analysis of the events in our sample we adopted the redshifts reported in Salvaterra et al. (2012). X-ray spectral indices are taken from Melandri et al. (2012) and hydrogen-equivalent column densities from Campana et al. (2012). Energetics and luminosities for the prompt emission are taken from Nava et al. (2012).

The best fit results, which are the base for our further analysis, are reported in Table 1, together with redshifts, hydrogen-equivalent column densities and spectral slopes.

3 RESULTS AND DISCUSSION

In Table 1 we report results obtained leaving the spectral slope of the optical/NIR data completely free or constraining this parameter to be in agreement with the results obtained by the analysis of simultaneous X-ray data. However, only in a minority of cases optical data alone allowed us to obtain useful estimates of the rest-frame extinction. In those cases results from both analyses are in reasonable agreement (Fig. 1). In the rest of the paper we will use only data obtained using the X-ray information.

Our sample consists of 58 events, covering the redshift range from ~ 0.1 to ~ 5.5 . Rest-frame extinctions or limits on it could be estimated for 53 events ($\sim 91\%$). For the remaining cases no information could be obtained due to the poor quality of optical data, X-ray data, or the lack of a redshift. In at least 8 cases ($\sim 15\%$) an extinction curve presenting a bump at $\sim 2175 \text{ \AA}$, i.e. LMC or MW, is required. Zafar et al. (2011), through GRB afterglow spectroscopy, measured this percentage to be about 7%, although in their sample high extinction events would likely be under-represented for observational biases. Broad-band photometry is clearly not the best tool to single out the extinction bump, in particular for low total extinction, and the true percentage is likely to be affected by the application of possible different extinction recipes (e.g. Calzetti et al. 1994;

⁵ <http://gcns.gsfc.nasa.gov/>

⁶ <http://www.python.org>

⁷ <http://www.scipy.org/SciPyPackages/Optimize>

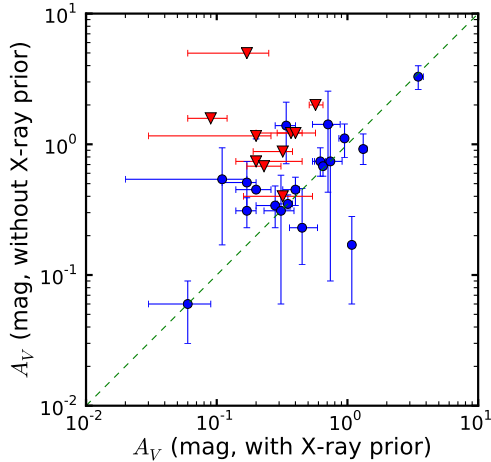


Figure 1. Comparison between A_V derived with and without assuming an X-ray prior. Only data for which at least one of the plotted quantities is not a limit are shown. Here and for later figures, blue (circle) symbols are actual measurements and red (triangles) symbols are upper or lower limits.

Maiolino et al. 2004; Liang & Li 2010). In a large fraction of cases, a chromatic extinction law is definitely required by the data.

The distribution of rest-frame extinctions is shown in Fig. 2 and resembles analogous histograms discussed by Kann et al. (2010) and Greiner et al. (2011). However, since our sample is selected with purely observational criteria of the prompt γ -ray emission, and it is highly complete in redshift, is likely to provide an unbiased view of the true “parent” distribution of rest-frame extinction for cosmological GRBs. The distribution seems to be bimodal, with a smooth distribution clustered at virtually zero extinction (including the upper limits) and several events (including the lower limits) at higher, roughly $A_V \geq 2$ mag, extinction. 87% of the GRB afterglows (46/53) have an extinction smaller than about 2 mag, and 50% smaller than 0.3–0.4 mag. The distribution is indeed strongly peaked at low extinction. The remaining 13% of events are on the contrary suffering from high extinction. They appear to follow, within the limits of the size of the sample, a different distribution being essentially inconsistent with a simple extrapolation of low-extinction events at more than 3σ level, if we model the low-extinction peak with a Gaussian or a Poissonian function. The percentage of events with large extinction could be even higher since the few events with no redshift measurements in our sample are likely part of this class. The true percentage of GRB afterglows showing high extinction is therefore probably between 15–20%, well in the range of the estimated percentage of dark bursts derived by means of different criteria and in different samples (de Pasquale et al. 2003; Jakobsson et al. 2004; Rol et al. 2005; van der Horst et al. 2009; Greiner et al. 2011; Melandri et al. 2012).

The shape of the low-extinction event distribution is roughly consistent with what could be expected in typical Galactic molecular clouds, although the amount of extinction is substantially lower than expected (e.g. Reichart & Price 2002; Vergani et al. 2004). The 15–20% of events with high extinction could be part of a different population of

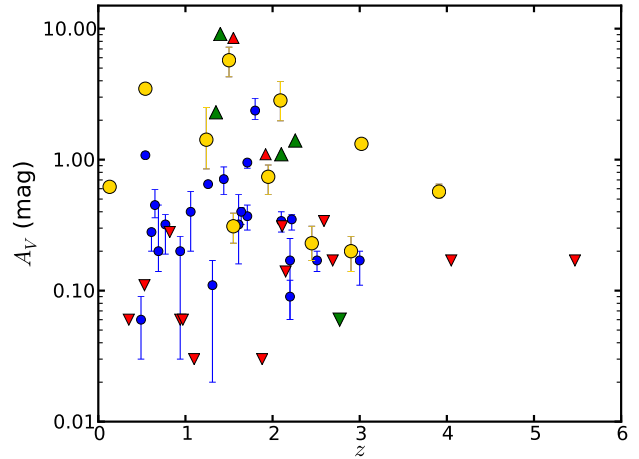


Figure 3. Extinction versus redshift. No clear relation appears to be present in the redshift range covered by our sample, although the largest extinctions are at $z \sim 1.5 - 2$, close to the expected peak of the star formation rate ($z \sim 2 - 3$, Hopkins & Beacom 2006). Bigger symbols (gold: measurements, green: limits) show data for dark bursts in our sample according to Melandri et al. (2012).

GRBs born in very dusty molecular clouds (Prochaska et al. 2009; Perley et al. 2009) and/or hosted by dusty, more massive, galaxies than the average of the host GRB population (e.g. Krühler et al. 2011; Rossi et al. 2012; Perley et al. 2013).

The derived rest-frame extinctions do not show a clear redshift dependence at least up to $z \sim 4$, where we have a sufficient number of events (Fig. 3). The most stringent upper limits are at low redshift, but this is probably an observational bias since the best optical data are found for those events. The largest extinctions are however at $z \sim 1.5 - 2$, close to the expected peak of the star formation rate ($z \sim 2 - 3$, Hopkins & Beacom 2006). This might have interesting consequences although the observed extinction in GRB afterglows is related to their LOSs and their physical properties do not necessarily correlate with global properties of their host galaxies. In the same plot we show the position in the A_V vs z plane of the dark bursts in our sample (Melandri et al. 2012). It is clear that, as expected, most dark bursts are characterized by a substantial optical extinction, in agreement with previous studies (e.g. Greiner et al. 2011; Krühler et al. 2011). An interesting exception is provided by GRB 081222 that is classified as dark (Melandri et al. 2012). Yet, it seems to be characterized by a very low dust extinction although the classification of this event as dark is questionable, as discussed in Melandri et al. (2012). On the contrary, GRB 060306 is characterized by a high extinction and it was not classified as dark. For this event only upper limits in the NIR are available (see Appendix A), and therefore even its classification is very uncertain. In any case, the classification of an event as dark always requires a careful comparison between optical and X-ray emission, and therefore the amount of optical extinction is only one of the important factors involved in the classification.

The relation between A_V and N_H derived by X-ray analysis has been widely discussed in the literature (e.g. Stratta

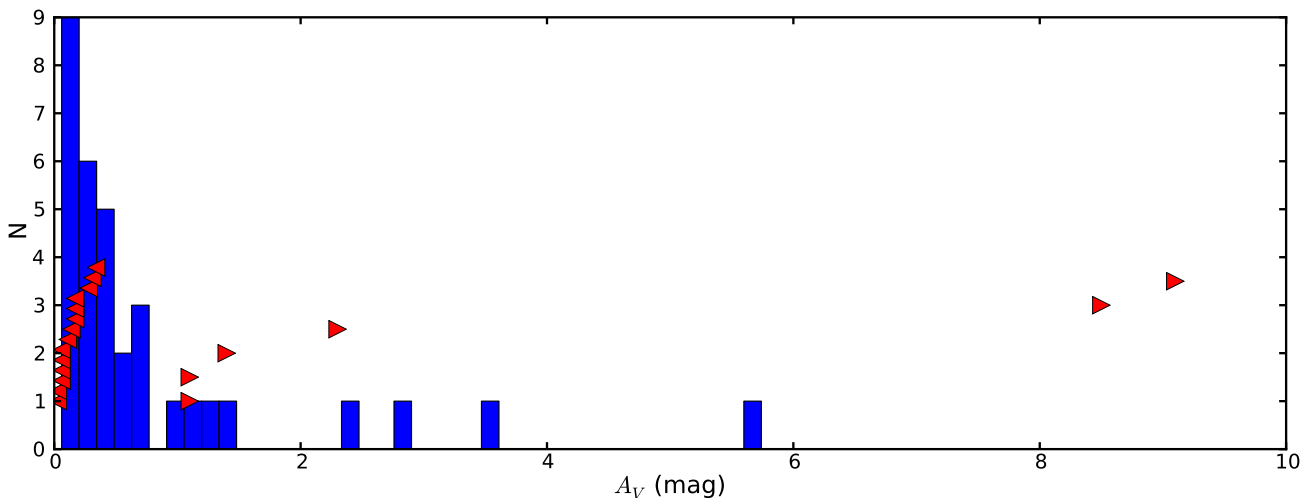


Figure 2. Histogram of the computed rest-frame A_V . Upper and lower limits are also reported. 87% of the GRB afterglows suffer from an extinction lower than about 2 mag, and 50% lower than 0.3-0.4 mag. About 13% of the population is characterized by a large extinction.

et al. 2004; Watson et al. 2007; Schady et al. 2010; Zafar et al. 2011; Watson et al. 2013). Taking into account the metallicity effect on the observed hydrogen-equivalent column densities there is a general consensus about a low dust-to-gas ratio ($\sim 10\%$) compared to typical Local Group (LG) values. Our sample (Fig. 4) indeed singles out a well defined trend with the highest rest-frame extinctions derived for the highest hydrogen-equivalent absorptions, roughly following the relation $N_H/A_V \sim 1.6 \times 10^{22} \text{ cm}^{-2} \text{ mag}^{-1}$. The typical LG dust-to-gas ratio (Welty et al. 2012) for Solar metallicity is also shown. Nonetheless, up to $A_V \sim 1$ mag the trend is not evident and there is a scattered distribution. The hint for two populations found from the A_V distribution (Fig. 2) might be found also in the N_H/A_V plan. The most absorbed afterglows (with $A_V \geq 1$ mag) are all characterized by the highest N_H values, i.e. larger than 10^{22} cm^{-2} .

Hydrogen-equivalent column densities derived through analysis of GRB afterglow X-ray data are actually due to photoelectric absorption by inner shells of elements as O, Si, S, Fe and He (see Watson et al. 2013, and references therein). The relation with hydrogen is obtained typically assuming a gas composition in Solar proportion and Solar metallicity. The comparison with dust absorption depends also on the dust-to-metal ratio (e.g. Savaglio et al. 2003; Zafar & Watson 2013). None of these parameters can, in general, be robustly determined by observations or predicted theoretically for the whole sample, making any firm inference about the relation between the X-ray N_H and A_V still difficult. Dust sublimation by the GRB emission (e.g. Waxman & Draine 2000) is usually invoked as a possible explanation for the low dust content along GRB LOSs, while the effect on the measured N_H can be less important since (mildly) ionized metals can still produce absorption in low-resolution soft X-ray spectra (e.g. Perna et al. 2003). However, as shown in Fig. 5, the energetics or luminosity of the GRB is not correlated with the amount of dust absorption, as it could be expected in case of sizable dust sublimation.

Watson et al. (2013) reported an evolution in redshift for the N_H/A_V relation, with higher values at high redshifts.

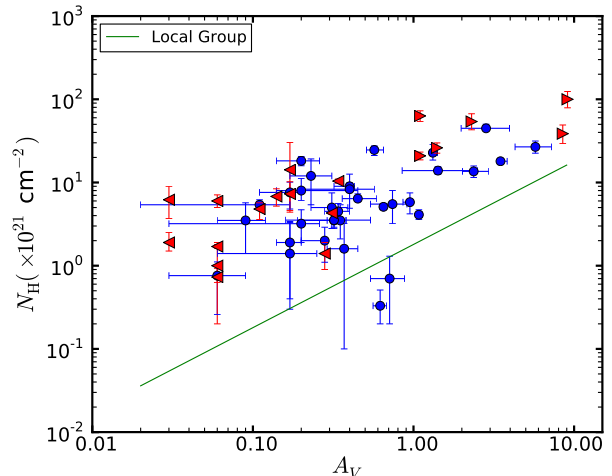


Figure 4. Relation between A_V and N_H derived by X-ray analysis. Typical dust-to-gas ratio for LG environments is also shown. Only data for which at least one of the plotted quantities is not a limit have been shown. No correction for metallicity different from Solar was applied to the observed N_H .

Based on our sample (Fig. 6) we can say that this is a direct consequence of lack of low N_H values at high redshift (see Campana et al. 2010, 2012), whereas A_V does not evolve with redshift (see Fig. 3). The physical reason of the preference for high N_H values at high redshifts and its significance have still to be determined.

In Campana et al. (2012) this phenomenon is attributed to the increasing absorption by intervening systems in higher redshift GRBs and therefore it would not be related to the progenitor environment (see, however, Watson et al. 2013 and Starling et al. 2013). The effect is important. The N_H contribution due to intervening systems, derived by a rough estimate from, e.g. Fig. 2 in Campana et al. (2010), at $z \sim 3$ is $\sim 6 \times 10^{20} \text{ cm}^{-2}$ and at $z \sim 6$ rises to $\sim 2 \times 10^{22} \text{ cm}^{-2}$. The subtraction of this contribution from

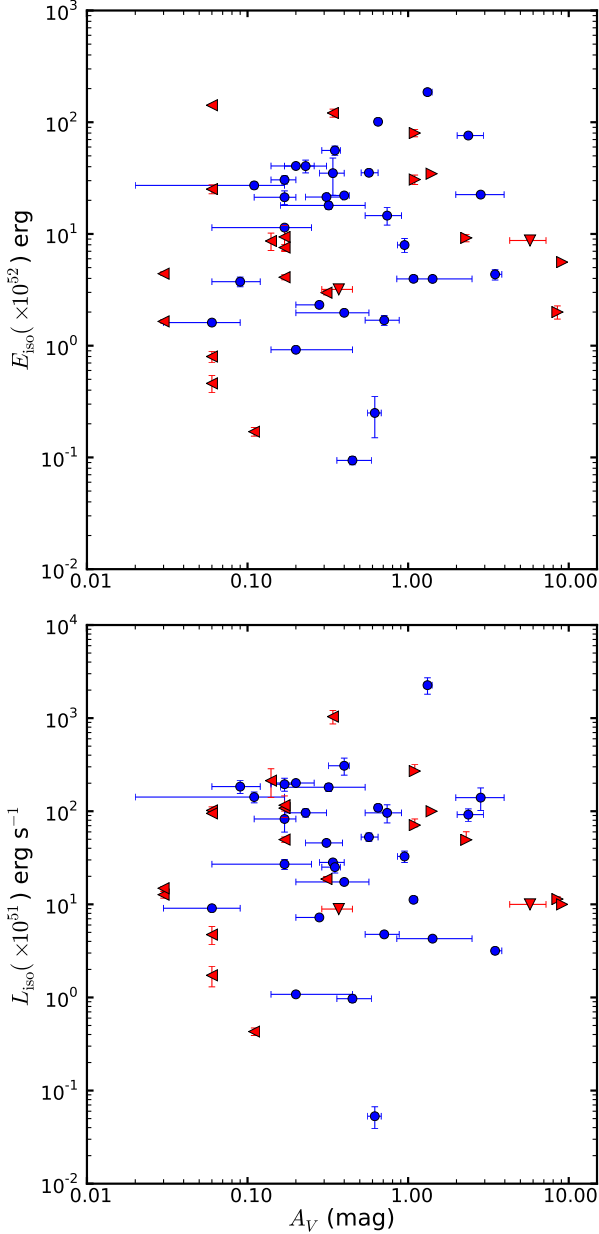


Figure 5. Extinction versus E_{iso} (upper panel) and L_{iso} (lower panel). The amount of extinction does not seem to be affected by the energetics or luminosity of the GRB.

the measured hydrogen-equivalent column densities does not however make the relation with the optical extinction more defined. The intrinsic uncertainties in deriving this relation added to the uncertainties associated to the derived N_{H} make it actually difficult to derive firmer conclusions.

The hydrogen column density can also be measured more directly when Lyman- α is visible in GRB afterglow spectra. This practically requires that events be at a redshift sufficiently high to have the Lyman- α transition in the useful spectral range of ground-based instruments, i.e. from the ultraviolet atmospheric cutoff at $\sim 3500 \text{ \AA}$ upwards. The redshift limit therefore is approximately $z > 2$. This limits

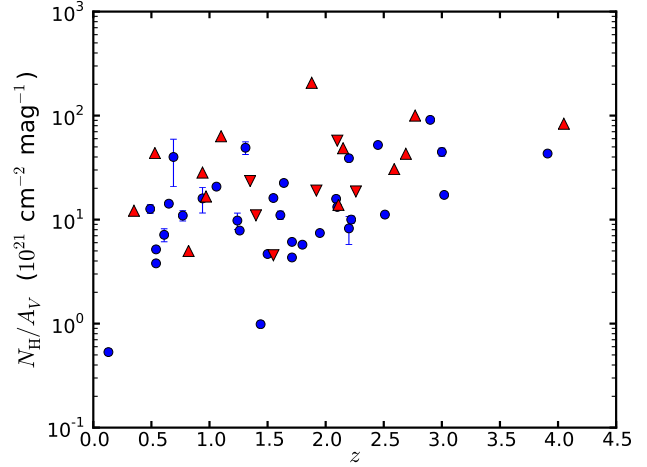


Figure 6. $N_{\text{H}}/A_{\text{V}}$ ratio versus redshift. A lack of low hydrogen-equivalent column densities at high redshifts mimics an increase of $N_{\text{H}}/A_{\text{V}}$ (see Campana et al. 2010, 2012).

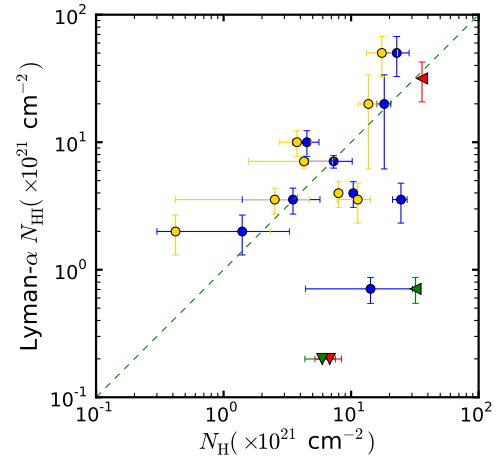


Figure 7. Relation between N_{H} from X-ray spectral analysis and N_{HI} derived by measuring Lyman- α . Blue and red symbols are as in Fig. 1. Gold and green symbols are measurements and upper limits after subtracting from the X-ray hydrogen-equivalent column density a contribution from intervening systems (see Campana et al. 2012).

the number of events for which Lyman- α has been measured. In our sample there are just 11 such events. Data are from Fynbo et al. (2009, and references therein) but for GRB081203A (Kuin et al. 2009). In Fig. 7 we show the relation between N_{H} based on Lyman- α observation (N_{HI}) and N_{H} based on X-ray analysis. If both N_{HI} and the gas responsible for the X-ray absorption come from the diffuse interstellar medium of the host galaxy, the two values should be correlated. For some of the events in our sample, rather surprisingly, the agreement is satisfactory. Possibly, for the sub-sample of events with both measurements, metallicity effects on the observed X-ray based N_{H} are not dominant. Nonetheless, as already discussed, the X-ray values are calculated using Solar metallicity, which might not correspond to the host metallicity, and past studies using larger sam-

ples found an excess of the X-ray hydrogen-equivalent column density compared to N_{HI} . It is interesting to note that if we again subtract to the X-ray values the mean contribution in the observed column density resulting from intervening systems as a function of redshift as empirically calculated by Campana et al. (2012), the relation between N_{H} and N_{HI} does become tighter (see Fig. 7), as expected if the gas responsible for both absorptions comes only from the GRB host. This can be a further hint, within the limits of the small available sample, for a possible contribution of the intervening systems to the hydrogen-equivalent column density determined from the X-ray.

4 CONCLUSIONS

In this paper we have computed rest-frame extinctions for a sample complete in redshift of GRBs (Salvaterra et al. 2012). The selection criteria of the sample rely only on observational high-energy parameters of the prompt emission and therefore our sample is not biased against dusty sight-lines. It is expected that our inferences hold for the general population of GRBs.

Our main result is that the extinction suffered by the analyzed GRBs does not seem to follow a single distribution. 87% of the events are absorbed by less than about 2 magnitudes, and 50% only suffer from less than 0.3-0.4 mag extinction. 13% of the events are instead more absorbed, and this population of GRBs may be due to highly dusty molecular clouds/star forming regions associated with the γ -ray burst progenitor or along the afterglow line of sight, and/or to massive dusty host galaxies. The true percentage of GRB afterglows showing high absorption is probably higher, since most of the events without reliable redshift measurements are likely part of this class.

No clear evolution in the dust extinction properties is evident within the redshift range of our sample ($\sim 0.1-5.5$), although the largest extinctions are at $z \sim 1.5-2$, close to the expected peak of the star formation rate ($z \sim 2-3$, Hopkins & Beacom 2006). Those GRBs classified as dark (Melandri et al. 2012) show higher than average extinction, confirming past claims about the nature of under luminous optical afterglows. There is a well defined relation between optical/NIR extinction and X-ray hydrogen-equivalent column density, although with a gas-to-dust ratio well above that observed in LG environments. Dust extinction does not seem to correlate with GRB energetics or luminosity, as it could be expected if dust properties are affected by the photon flux from the high-energy event.

ACKNOWLEDGMENTS

This work has been supported by ASI grant I/004/11/0 and by PRIN-MIUR 2009 grants. The Dark Cosmology Centre is funded by the Danish National Research Foundation. This research has made use of the APASS database, located at the AAVSO web site. Funding for APASS has been provided by the Robert Martin Ayers Sciences Fund. S.C. thanks Cristiano Guidorzi for enlightening discussions and Paul Kuin for having provided data in a suitable format for analysis. A.G. acknowledges funding from the Slovenian Research

Agency and from the Centre of Excellence for Space Science and Technologies SPACE-SI, an operation partly financed by the European Union, the European Regional Development Fund, and the Republic of Slovenia. We thank the referee, Bruce Gendre, for his useful comments.

REFERENCES

- Alatalo A.J., Perley P., & Bloom J.S., 2006, GCN 4702
- Aoki K., Totani T., Hattori T., Ohta K., Kawabata K., Kobayashi N., Iye M., Nomoto K., & Kawai N., 2009, PASP, 61, 387
- Berger E., et al., 2005, ApJ, 634, 501
- Berger E., & Gonzalez S., 2007, GCN 7104
- Blustin A.J., et al., 2006, ApJ, 637, 901
- Bloom J.S., Perley D.A., & Starr D.L., 2007, GCN 6953
- Bloom J.S., et al., 2007, GCN 7105
- Bloom J.S., et al., 2007, GCN 7110
- Bloom J.S., et al., 2009, ApJ, 691, 723
- Breeveld A., et al., 2008, GCN 8712
- Calzetti D., Kinney A.L., & Storchi-Bergmann T., 1994, ApJ, 429, 229
- Campana S., et al., 2010, MNRAS, 402, 2429
- Campana S., et al., 2012, MNRAS, 421, 1697
- Cash W., 1976, A&A, 52, 307
- Cenko, S.B. et al., 2006a, GCN 5457
- Cenko, S.B. et al., 2006b, GCN 5975
- Cenko, S.B. et al., 2006c, GCN 5978
- Cenko S.B., Kelemen J., Harrison F.A., Fox D.B., Kulkarni S.R., Kasliwal M.M., Ofek E.O., Rau A., Gal-Yam A., Frail D.A., & Moon D.-S., 2009, ApJ, 693, 1484
- Cenko S.B., et al., 2010, AJ, 140, 224
- Chen S.L., Li A. & Wei D.M., 2006b, ApJ, 647, 13
- Chen H.-W., et al., 2006a, GCN 4861
- Cobb B.E., 2009, GCN 9313
- Cobb B.E., 2010, ApJ, 718, 150
- Covino S., et al., 2005, GCN 4046
- Covino S., et al., 2008, MNRAS, 388, 347
- Covino S., et al., 2008b, GCN 8692
- Covino S., et al., 2010, A&A, 521, 53
- Cucchiara A., et al., 2011, ApJ, 743, 154
- Curran P., et al., 2007a, MNRAS, 381, 65
- Curran P., et al., 2007b, A&A, 467, 1049
- Curran P., et al., 2009, GCN 8770
- Davanzo P., et al., 2009, GCN 8873
- Davanzo P., et al., 2012, MNRAS, 425, 506
- D'Elia V. et al., 2010, A&A, 523, 36
- D'Elia V. & Stratta G., 2011, A&A, 532, 48
- de Pasquale M., et al., 203, ApJ, 592, 1018
- de Pasquale M., et al., 2006a, MNRAS, 365, 1031
- de Pasquale M., et al., 2006b, GCN 4852
- de Pasquale M., et al., 2008, GCN 8603
- de Pasquale M., et al., 2009, GCN 10267
- Della Valle M., et al., 2006, Nature, 444, 1050
- Deng J., Zheng W., Zhai M., Xin L., Qiu Y., Stefanescu A., Pozanenko A., Ibrahimov M. & Volnova A., 2009, ApJ, submitted (arXiv:0912.5435)
- Draine B.T. & Hao L., 2002, ApJ, 569, 780
- Fatkhullin T., et al., 2008, GCN 8695
- Filgas R., et al., 2011a, A&A, 526, 113
- Filgas R., et al., 2011b, A&A, 535, 57

Table 1. Spectral and absorption parameters for GRBs in our sample. For each event we list the redshift, the X-ray spectral index, the X-ray hydrogen-equivalent absorbing column, the optical/NIR spectral index and the amount of rest-frame reddening in the visual band.

Event	z	β_X	N_H 10^{21} cm^{-2}	β_o	No X-ray prior		With X-ray prior		
					A_V	Ext. curve	β_o	A_V	Ext. curve
GRB 050318	1.44	$0.95^{+0.07}_{-0.06}$	$0.7^{+0.6}_{-0.5}$	$-2.00^{+3.89}_{-4.90}$	$1.42^{+1.13}_{-0.99}$	SMC	$0.89^{+0.13}_{-0.00}$	$0.71^{+0.17}_{-0.17}$	SMC
GRB 050401	2.90	$0.83^{+0.15}_{-0.14}$	$18.2^{+2.3}_{-2.3}$	$-0.42^{+0.65}_{-0.73}$	$0.45^{+0.28}_{-0.25}$	SMC	$0.19^{+0.29}_{-0.00}$	$0.20^{+0.06}_{-0.11}$	SMC
GRB 050416A	0.65	$1.11^{+0.11}_{-0.15}$	$6.4^{+0.9}_{-0.9}$	$1.04^{+0.25}_{-0.33}$	$0.23^{+0.23}_{-0.11}$	SMC	$0.72^{+0.00}_{-0.17}$	$0.45^{+0.14}_{-0.09}$	SMC
GRB 050525A	0.61	$1.08^{+0.13}_{-0.13}$	$2.0^{+0.9}_{-0.9}$	$0.27^{+0.48}_{-0.52}$	$0.34^{+0.14}_{-0.11}$	SMC	$0.45^{+0.28}_{-0.00}$	$0.28^{+0.00}_{-0.08}$	SMC
GRB 050802	1.71	$0.89^{+0.04}_{-0.07}$	$1.6^{+1.6}_{-1.5}$	$0.34^{+1.10}_{-1.42}$	< 1.22	SMC	$0.34^{+0.09}_{-0.02}$	$0.37^{+0.08}_{-0.08}$	SMC
GRB 050922C	2.20	$1.25^{+0.06}_{-0.07}$	$3.5^{+2.2}_{-2.1}$	$-0.30^{+1.47}_{-4.74}$	< 1.58	SMC	$0.68^{+0.13}_{-0.00}$	$0.09^{+0.03}_{-0.03}$	SMC
GRB 060206	4.05	$1.30^{+0.57}_{-0.53}$	$14.2^{+16.0}_{-9.8}$	$0.46^{+0.41}_{-0.39}$	< 0.25	SMC	$0.46^{+0.41}_{-0.19}$	< 0.17	SMC
GRB 060210	3.91	$1.08^{+0.05}_{-0.05}$	$24.6^{+2.9}_{-3.5}$	$4.47^{+0.28}_{-9.51}$	< 2.00	SMC	$1.13^{+0.00}_{-0.10}$	$0.57^{+0.08}_{-0.06}$	SMC
GRB 060306	1.55 ^a	$1.62^{+0.28}_{-0.26}$	$38.6^{+10.5}_{-9.1}$				0.86	> 8.5	SMC
GRB 060614	0.13	$0.89^{+0.06}_{-0.04}$	$0.33^{+0.18}_{-0.13}$	$0.18^{+0.20}_{-0.23}$	$0.74^{+0.20}_{-0.17}$	SMC	$0.35^{+0.09}_{-0.00}$	$0.62^{+0.06}_{-0.06}$	SMC
GRB 060814	1.92	$1.13^{+0.07}_{-0.07}$	$20.9^{+2.3}_{-2.2}$				0.56	> 1.1	SMC
GRB 060904A		$0.28^{+0.74}_{-0.47}$	> 2.07						
GRB 060908	1.88	$1.42^{+0.32}_{-0.36}$	$6.2^{+2.8}_{-2.5}$	$0.22^{+0.22}_{-0.26}$	< 0.20	SMC	$0.56^{+0.02}_{-0.00}$	< 0.03	SMC
GRB 060912A	0.94	$0.71^{+0.19}_{-0.33}$	$3.2^{+1.5}_{-1.3}$	$-0.08^{+1.23}_{-1.42}$	< 1.16	SMC	$0.46^{+0.44}_{-0.00}$	$0.20^{+0.06}_{-0.17}$	SMC
GRB 060927	5.47	$0.96^{+0.33}_{-0.25}$	< 36	$0.75^{+0.41}_{-2.35}$	< 1.33	SMC	$0.75^{+0.00}_{-0.04}$	< 0.17	SMC
GRB 061007	1.26	$1.01^{+0.09}_{-0.06}$	$5.1^{+0.3}_{-0.3}$	$0.87^{+0.27}_{-0.24}$	$0.68^{+0.08}_{-0.11}$	LMC	$0.97^{+0.13}_{-0.02}$	$0.65^{+0.03}_{-0.03}$	LMC
GRB 061021	0.35	$1.00^{+0.04}_{-0.05}$	$0.73^{+0.2}_{-0.1}$	$0.04^{+0.42}_{-0.60}$	< 0.42	SMC	$0.45^{+0.09}_{-0.00}$	< 0.06	SMC
GRB 061121	1.31	$0.91^{+0.06}_{-0.06}$	$5.4^{+0.8}_{-0.5}$	$-1.15^{+1.21}_{-1.41}$	$0.54^{+0.40}_{-0.37}$	SMC	$0.35^{+0.12}_{-0.00}$	$0.11^{+0.06}_{-0.09}$	SMC
GRB 061122A	2.09	$0.95^{+0.07}_{-0.06}$	$44.8^{+5.4}_{-3.0}$				$0.45^{+0.07}_{-0.06}$	$2.83^{+1.13}_{-0.85}$	SMC
GRB 070306	1.50	$0.95^{+0.07}_{-0.06}$	$26.8^{+4.7}_{-4.3}$				$0.39^{+0.13}_{-0.00}$	$5.74^{+1.48}_{-1.45}$	SMC
GRB 070328	< 4	$0.95^{+0.08}_{-0.08}$							
GRB 070521	1.35	$1.03^{+0.15}_{-0.13}$	54^{+13}_{-11}				0.40	> 2.3	SMC
GRB 071020	2.15	$0.89^{+0.16}_{-0.14}$	$6.8^{+1.6}_{-1.6}$	$0.58^{+0.28}_{-1.71}$	< 1.13	SMC	$0.75^{+0.20}_{-0.00}$	< 0.14	SMC
GRB 071112C	0.82	$0.79^{+0.21}_{-0.27}$	$1.4^{+0.5}_{-0.5}$	$0.48^{+0.19}_{-0.37}$	< 0.28	SMC	$0.49^{+0.01}_{-0.37}$	< 0.28	SMC
GRB 071117	1.33	$1.09^{+0.13}_{-0.19}$	$10.9^{+2.1}_{-3.1}$						
GRB 080319B	0.94	$0.82^{+0.06}_{-0.06}$	$1.7^{+0.1}_{-0.1}$	$0.22^{+0.15}_{-0.15}$	$0.09^{+0.06}_{-0.06}$	SMC	$0.26^{+0.10}_{-0.00}$	< 0.06	SMC
GRB 080319C	1.95	$0.97^{+0.28}_{-0.23}$	$5.5^{+2.5}_{-2.3}$	$0.48^{+1.66}_{-1.64}$	$0.74^{+0.65}_{-0.65}$	SMC	$0.48^{+0.27}_{-0.24}$	$0.74^{+0.17}_{-0.20}$	SMC
GRB 080413B	1.10	$0.97^{+0.05}_{-0.07}$	$1.9^{+0.6}_{-0.4}$	$0.13^{+0.08}_{-0.08}$	$0.11^{+0.03}_{-0.03}$	SMC	$0.40^{+0.01}_{-0.00}$	< 0.03	SMC
GRB 080430	0.77	$1.06^{+0.06}_{-0.07}$	$3.5^{+0.8}_{-0.6}$	$0.50^{+0.95}_{-1.27}$	< 0.88	LMC	$0.49^{+0.13}_{-0.00}$	$0.32^{+0.06}_{-0.13}$	LMC
GRB 080602	1.40	$0.90^{+0.12}_{-0.13}$	$6.7^{+2.4}_{-2.1}$						
GRB 080603B	2.69	$0.87^{+0.26}_{-0.21}$	$7.3^{+2.9}_{-2.7}$	$0.22^{+0.55}_{-0.74}$	< 0.45	SMC	$0.19^{+0.44}_{-0.03}$	< 0.17	SMC
GRB 080605	1.64	$0.86^{+0.11}_{-0.16}$	$9.0^{+0.9}_{-0.9}$	$0.65^{+0.24}_{-0.22}$	$0.45^{+0.11}_{-0.11}$	SMC	$0.74^{+0.20}_{-0.04}$	$0.40^{+0.03}_{-0.08}$	SMC
GRB 080607	3.02	$1.13^{+0.06}_{-0.11}$	$22.8^{+5.7}_{-4.2}$	$1.73^{+0.27}_{-0.29}$	$0.92^{+0.28}_{-0.22}$	MW	$1.19^{+0.00}_{-0.11}$	$1.32^{+0.09}_{-0.06}$	MW
GRB 080613B		$1.39^{+1.28}_{-0.87}$	> 0.5						
GRB 080721	2.59	$0.91^{+0.05}_{-0.05}$	$10.4^{+0.6}_{-0.6}$	$-4.13^{+5.13}_{-7.30}$	< 2.97	SMC	$0.86^{+0.10}_{-0.00}$	< 0.34	SMC
GRB 080804	2.20	$0.97^{+0.12}_{-0.12}$	$1.4^{+1.9}_{-1.1}$	$-8.45^{+10.10}_{-18.18}$	< 4.98	SMC	$0.37^{+0.22}_{-0.02}$	$0.17^{+0.08}_{-0.11}$	SMC
GRB 080916A	0.69	$1.07^{+0.13}_{-0.18}$	$8.0^{+3.2}_{-1.9}$	$1.47^{+0.09}_{-0.43}$	< 0.74	SMC	$1.20^{+0.00}_{-0.31}$	$0.20^{+0.25}_{-0.06}$	SMC
GRB 081007	0.53	$1.04^{+0.18}_{-0.18}$	$4.8^{+0.9}_{-1.2}$	$0.43^{+0.33}_{-0.38}$	$0.31^{+0.25}_{-0.23}$	SMC	$0.86^{+0.07}_{-0.00}$	< 0.11	SMC
GRB 081121	2.51	$0.95^{+0.08}_{-0.08}$	$1.9^{+1.6}_{-1.5}$	$-0.31^{+0.43}_{-0.41}$	$0.31^{+0.08}_{-0.08}$	SMC	$0.37^{+0.12}_{-0.00}$	$0.17^{+0.03}_{-0.03}$	SMC
GRB 081203A	2.10	$1.14^{+0.09}_{-0.10}$	$4.5^{+1.1}_{-1.0}$	$-5.92^{+4.18}_{-4.51}$	$1.39^{+0.71}_{-0.68}$	SMC	$0.67^{+0.12}_{-0.07}$	$0.34^{+0.06}_{-0.06}$	SMC
GRB 081221	2.26	$1.50^{+0.12}_{-0.11}$	$26.1^{+3.8}_{-3.6}$				0.89	> 1.4	SMC
GRB 081222	2.77	$1.03^{+0.07}_{-0.06}$	$6.0^{+1.1}_{-1.0}$	$-0.01^{+0.52}_{-0.54}$	< 0.54	SMC	$0.47^{+0.12}_{-0.00}$	< 0.06	SMC
GRB 090102	1.55	$0.78^{+0.06}_{-0.08}$	$5.0^{+2.5}_{-2.2}$	$0.27^{+0.54}_{-0.59}$	$0.31^{+0.27}_{-0.25}$	SMC	$0.27^{+0.09}_{-0.05}$	$0.31^{+0.08}_{-0.08}$	SMC
GRB 090201	2.1 ^b	$0.97^{+0.11}_{-0.10}$	$63.1^{+9.6}_{-8.9}$				0.49	> 1.1	SMC
GRB 090424	0.54	$0.95^{+0.10}_{-0.09}$	$4.1^{+0.6}_{-0.5}$	$1.41^{+0.20}_{-0.15}$	$0.17^{+0.11}_{-0.11}$	SMC	$0.55^{+0.00}_{-0.06}$	$1.08^{+0.06}_{-0.03}$	MW
GRB 090709A	1.80 ^c	$0.87^{+0.07}_{-0.07}$	$13.6^{+2.2}_{-2.1}$	$0.24^{+2.93}_{-7.48}$	< 15.8	LMC	$0.44^{+0.00}_{-0.14}$	$2.37^{+0.57}_{-0.35}$	LMC
GRB 090715B	3.0	$1.04^{+0.09}_{-0.09}$	$7.6^{+2.5}_{-2.8}$	$-1.09^{+0.85}_{-0.91}$	$0.51^{+0.23}_{-0.20}$	SMC	$0.45^{+0.00}_{-0.18}$	$0.17^{+0.03}_{-0.06}$	SMC
GRB 090812	2.45	$0.95^{+0.07}_{-0.06}$	$12.0^{+7.2}_{-6.6}$	$0.58^{+0.85}_{-1.01}$	< 0.68	SMC	$0.52^{+0.00}_{-0.13}$	$0.23^{+0.08}_{-0.06}$	SMC
GRB 090926B	1.24	$0.95^{+0.07}_{-0.06}$	$13.9^{+1.6}_{-1.5}$					$(1.42^{+1.08}_{-0.57})^d$	SMC
GRB 091018	0.97	$1.18^{+0.18}_{-0.23}$	$1.0^{+0.9}_{-0.8}$	$0.57^{+0.01}_{-0.06}$	< 0.06	SMC	$0.57^{+0.01}_{-0.06}$	< 0.06	SMC

^a This redshift was revised by Jakobsson et al. (2012) and Perley et al. (2013).^b This redshift is reported in Krühler et al. (2013b).^c This redshift was revised by Perley et al. (2013).^d This figure is reported in Greiner et al. (2011), although the related photometry has not been published.

Table 1 – continued

GRB 091020	1.71	$1.11^{+0.05}_{-0.06}$	$5.8^{+1.7}_{-1.6}$	$0.23^{+0.65}_{-0.64}$	$1.11^{+0.32}_{-0.32}$	SMC	$0.55^{+0.11}_{-0.00}$	$0.95^{+0.03}_{-0.09}$	SMC
GRB 091127	0.49	$0.80^{+0.11}_{-0.11}$	$0.76^{+0.35}_{-0.50}$	$0.28^{+0.03}_{-0.02}$	$0.06^{+0.03}_{-0.03}$	SMC	$0.29^{+0.00}_{-0.04}$	$0.06^{+0.03}_{-0.03}$	SMC
GRB 091208B	1.06	$0.94^{+0.13}_{-0.08}$	$8.3^{+4.3}_{-3.4}$	$0.94^{+0.83}_{-1.19}$	< 1.22	SMC	$0.94^{+0.13}_{-0.08}$	$0.40^{+0.17}_{-0.20}$	SMC
GRB 100615A	1.40 ^e	$1.20^{+0.30}_{-0.28}$	$100^{+24.0}_{-21.0}$				0.76	> 9.1	SMC
GRB 100621A	0.54	$1.40^{+0.13}_{-0.12}$	$18.0^{+1.2}_{-1.1}$	$1.19^{+0.64}_{-0.65}$	$3.29^{+0.70}_{-0.66}$	LMC	$1.03^{+0.00}_{-0.25}$	$3.48^{+0.35}_{-0.09}$	LMC
GRB 100728B	2.11	$1.08^{+0.17}_{-0.18}$	$4.3^{+3.1}_{-2.5}$	$0.70^{+0.31}_{-0.46}$	< 0.48	SMC	$0.70^{+0.05}_{-0.30}$	< 0.31	SMC
GRB 110205A	2.22	$1.13^{+0.08}_{-0.09}$	$3.5^{+1.9}_{-1.4}$	$0.55^{+0.10}_{-0.12}$	$0.35^{+0.06}_{-0.03}$	LMC	$0.55^{+0.30}_{-0.01}$	$0.35^{+0.03}_{-0.06}$	LMC
GRB 110503A	1.61	$0.95^{+0.04}_{-0.06}$	$3.53^{+0.67}_{-0.64}$	$1.28^{+0.36}_{-0.74}$	< 0.40	SMC	$0.49^{+0.00}_{-0.10}$	$0.32^{+0.22}_{-0.16}$	LMC

^e This redshift is reported in Krühler et al. (2013a).

- Fynbo J.P.U., et al., 2009, ApJS, 185, 526
 Fruchter A., Krolik J.H. & Rhoads J.E., 2001, ApJ, 563, 597
 Gallerani S., et al. 2010, A&A, 523, 85
 Gehrels N., Ramirez-Ruiz E. & Fox D.B. 2009, ARA&A, 47, 567
 Gendre B., et al. 2010, MNRAS 405, 2372
 Gendre B., et al. 2012, ApJ 748, 59
 Ghirlanda G., et al. 2012, MNRAS 422, 2553
 Greco G., Terra F., Nanni D., Bartolini C., Guanrinieri A., Piccioni A., Pizzichini G., Gualandi R., 2006, GCN 4732
 Greiner J., et al. 2008, PASP, 120, 405
 Greiner J., et al. 2011, A&A, 526, 30
 Hopkins A.M. & Beacom J.F., 2006, ApJ, 651, 142
 Jakobsson P., et al. 2004, ApJ, 617, 21
 Jakobsson P., et al. 2007, GCN 7117
 Jakobsson P., et al. 2012, ApJ, 752, 62
 Jaunsen A.O., et al. 2008, ApJ, 681, 453
 Jélinek M., et al. 2012, AcPol, 52, 34
 Jin Z.P., et al. 2013, ApJ, *submitted*
 Haislip J., et al. 2006, GCN 4709
 Haislip J., et al. 2009, GCN 9927
 Henden A., et al., 2005, GCN 3855
 Holland S., et al. 2007, AJ, 133, 122
 Huang K.Y., et al. 2012, ApJ 748, 44
 Kamble A., Misra K., Bharracharya D., Sagar R., 2009, MNRAS, 394, 214
 Kann D.A., et al. 2009a, GCN 10076
 Kann D.A., et al. 2009b, GCN 10090
 Kann D.A., et al. 2010, ApJ, 720, 1513
 Kann D.A., et al. 2011, ApJ, 734, 96
 Krühler T., et al. 2011, A&A, 534, 108
 Krühler T., et al. 2012, ApJ 758, 46
 Krühler T., et al. 2013a, GCN 14264
 Krühler T., et al. 2013b, in preparation
 Kuin N.P.M., et al., 2008, GCN 7808
 Kuin N.P.M., et al., 2008b, GCN 8069
 Kuin N.P.M., et al., 2009, MNRAS 395, 21
 Kuroda, D., et al., 2011a, GCN 11651
 Kuroda, D., et al., 2011b, GCN 11652
 Lamb D.Q., et al., 2006, GCN 5079
 Landsman W.B. et al., 2008, GCN 7660
 Lazzati D., Covino S., & Ghisellini G., 2002, MNRAS, 330, 583
 Levan A.J., et al., 2006a, GCN 5455
 Levan A.J., et al., 2006b, GCN 5461
 Liang S.L. & Li E., 2010, ApJ, 710, 648
 Loew S., et al., 2008, GCN 8540
 Lü G.-J., Shao L., Jin Z.-P. & Wei D.-M., 2011, ChA&A 35, 372
 Maiolino R., et al., 2004, Nature, 431, 533
 Malesani D., et al., 2006b, GCN 5456
 Malesani D., et al., 2006a, GCN 4706
 Malesani D., et al., 2008a, GCN 7783
 Malesani D., et al., 2008b, GCN 8688
 Mangano V., et al., 2007, A&A, 470, 105
 Marshall F.E., et al., 2007, GCN 6229
 Melandri A., et al., 2012, MNRAS, 421, 1265
 Miller A.A., et al., 2008, GCN 7827
 Minezaki T., et al., 2007, GCN 6456
 Monfardini A., et al., 2006, ApJ, 648, 1125
 Morgam A. & Bloom J.S., 2011, GCN 11998
 Mundell C.G. et al., 2007, ApJ 660, 489
 Naito H. et al., 2010, GCN 10881
 Nava L., et al., 2012, MNRAS, 421, 1256
 Nysewander M., et al., 2006, GCN 4857
 Oates S.R., et al., 2007a, MNRAS, 395, 490
 Oates S.R., et al., 2007b, GCN 7080
 Oates S.R., et al., 2008, GCN 8249
 Oates S.R., et al., 2008b, GCN 8544
 Oates S.R., et al., 2009, MNRAS, 395, 490
 Oates S.R., et al., 2009b, GCN 10054
 Oates S.R., et al., 2010, GCN 11026
 Oates S.R., et al., 2011, GCN 12000
 Olivares F., et al., 2009, GCN 9245
 Olivares F., et al., 2010, GCN 11013
 Pandey S.B., et al., 2009, A&A, 504, 45
 Pei Y.C., 1992, ApJ, 138, 1690
 Perley D.A., et al. 2009, AJ, 138, 1690
 Perley D.A., et al. 2011, AJ, 141, 36
 Perley D.A., et al. 2013, ApJ submitted (arXiv:1301:5903)
 Perna R. & Lazzati D., 2002, ApJ, 580, 261
 Perna R., Lazzati D. & Fiore F., 2003, ApJ, 585, 775
 Piran T., 2004, RvMP, 76, 1143
 Price P.A. , et al., 2005, GCN 3312
 Prochaska J.X., et al., 2009, ApJ 691, 27
 Racusin J., et al., 2008, Nature, 455, 183
 Racusin J., et al., 2009, GCN Rep 257
 Reichart D.E. & Price P.A., 2002, ApJ, 565, 174
 Resmi L., et al., 2012, MNRAS 427, 288
 Rol E., et al., 2005, ApJ, 624, 868
 Rossi A., et al., 2012, A&A, 545, 77
 Ruiz-Velasco A.E., et al., 2007, ApJ, 669, 1
 Rykoff E.S., et al., 2005, ApJ, 631, 121

Salvaterra R., et al., 2012, ApJ, 749, 68
 Sari R., Piran T. & Narayan R., 1998, ApJ, 497, 17
 Savaglio S., Fall S. M., & Fiore F., 2003, ApJ, 585, 638
 Schady P., et al. 2007, MNRAS, 377, 273
 Schady P., et al. 2008, GCN 7858
 Schady P., et al. 2009, GCN 9774
 Schady P., et al. 2010, MNRAS, 401, 2773
 Schady P., et al. 2012, A&A, 537, 15
 Schlegel D. J., Finkbeiner D.P., & Davis M., 1998, ApJ, 500, 525
 Schulze S., et al., 2011, A&A, 526, 23
 Soderberg A., et al., 2007, ApJ, 661, 982
 Stanek K.Z., et al., 2007, ApJ, 654, 21
 Starling R.L.C., et al., 2009, MNRAS, 400, 90
 Starling R.L.C., et al., 2013, MNRAS, in press (arXiv:1303.0844)
 Still M., et al., 2005, ApJ, 635, 1187
 Stratta G., et al., 2004, ApJ, 608, 846
 Terada H., Pyo T.-S., Kobayashi N., Kawai N., 2006, GCN 4716
 Testa et al., 2005, GCN 3765
 Uehara T., et al., 2010, A&A, 519, 56
 Uhm Z.L. & Zhang B., 2013, ApJ, submitted (arXiv:1301.0291)
 Updike et al., 2008, GCN 8693
 Updike et al., 2009, GCN 9773
 Updike et al., 2009b, GCN 10271
 Urata et al., 2011, GCN 11648
 van der Horst A.J., et al., 2009, ApJ 699, 1087
 Vergani S., et al., 2004, A&A 415, 171
 Vergani S., et al., 2011, A&A 535, 57
 Vernet J., et al., 2011, A&A 536, 105
 Volnova, A., et al., 2010, GCN 11045
 Watson D., et al., 2006, ApJ, 652, 1011
 Watson D., et al., 2007, ApJ, 660, 101
 Watson D., et al., 2013, ApJ, submitted (arXiv:1212.4492)
 Watson D. & Jakobsson P., 2012, ApJ 754, 89
 Waxman E. & Draine B.T., 2000, ApJ, 537, 796
 Welty D.E., Xue R. & Wong T., 2012, ApJ, 745, 173
 Wiersema K., 2011, AN, 332, 295
 Wiersema K., et al., 2012, MNRAS, MNRAS 426, 2
 Woźniak P.R., Vestrand W.T., Wren J.A., White R.R., Evans S.M. & Caspersen D., 2006, ApJ, 642, 99
 Xu D. et al., 2009, GCN 9941
 Zafar T. et al., 2012, ApJ, 753, 82
 Zafar T., Watson D., Fynbo J.P.U., Malesani D., Jakobsson P. & de Ugarte Postigo A., 2011, A&A, 532, 143
 Zafar T. & Watson T., 2013, A&A, submitted (arXiv:1303.1141)
 Zhang B., & Mészáros P. 2004, IJMPA, 19, 2385
 Zheng, W., et al. 2012, ApJ, 751, 90
 Ziaepour H., et al. 2008, GCN 167, 3

APPENDIX A: GRBS ANALYSED IN OUR SAMPLE

In this section we will frequently refer to various photometric bands. With capital letters we refer to the Johnson-Morgan-Cousin bands: U, B, V, R_c, I_c . With primed small letters

we refer to the SDSS photometric system u', g', r', i', z' ⁶. *Swift*-UVOT bands are again referred with lower-case letters $uvw2, uvm2, uvw1, u, b, v, wh$. In a few cases systematic errors to bring the fit quality to a level adequate for error modeling were introduced. Which data were selected from the literature and specific comments are reported below for each analyzed event.

GRB 050318 *Swift*-UVOT u, b and v (AB) magnitudes, reported in Still et al. (2005), and an R_c band measurement, reported by Berger et al. (2005), are available. Calibrations of these two datasets do not appear to be in agreement, and therefore we neglected the R_c point.

GRB 050401 We collected data from Rykoff et al. (2005); de Pasquale et al. (2006); Watson et al. (2006); Kamble et al. (2009) in the V, R_c, I_c, J, H and K bands. However, according to the authors, R band data in de Pasquale et al. (2006) are poorly calibrated and have not been used in the analyses. In addition R band data in Watson et al. (2006) and Kamble et al. (2009) are in strong disagreement. Given the more detailed calibration process reported by Kamble et al. (2009) we chose to use these data.

GRB 050416A We collected data from Holland et al. (2007); Soderberg et al. (2007) and Price et al. (2005) in the *Swift*-UVOT $uvm2, u, b, v$ and R_c, I_c, z and K bands. From this dataset we did not consider the GCN data due to the very preliminary calibration and one I point in Holland et al. (2007) at about 1150 min that was clearly discrepant. We also removed *Swift*-UVOT data with error larger than 0.4 mag.

GRB 050525A This event was observed intensively. We collected *Swift*-UVOT data in the $uvw2, w1, u, b, v$ bands from Blustin et al. (2006). We neglected all data with calibration based only on preliminary photometry.

GRB 050802 We collected data from Oates et al. (2007a) in the *Swift*-UVOT $uvw1, u, b, v$ bands and from Table A1 in the u', B, V, R_c and I_c bands. In Testa et al. (2005) preliminary TNG⁷ photometry was reported. Here we re-calibrated all the available data following the field calibration by Henden et al. (2005) for BVR_cI_c and SDSS⁸ photometry for u' . We neglected *Swift*-UVOT data obtained after about 8 hr after the GRB and magnitudes with errors larger than 0.4 mag. In any case *Swift*-UVOT still shows a considerable scatter, likely intrinsic, and to obtain a satisfactory fit we had to introduce a 15% systematic error to be added in quadrature.

GRB 050922C We collected data from Oates et al. (2009) in the *Swift*-UVOT u, b, v bands. In Table A2 we report VLT⁹ photometry in B, V and R_c bands calibrated by Landolt standard field stars and preliminarily published in

⁶ <http://www.sdss.org/>

⁷ <http://www.tng.iac.es/>

⁸ <http://skyserver.sdss3.org/dr8/en/>

⁹ <http://www.eso.org/>

Table A1. TNG data for GRB 050802. u' magnitude is in the AB system, BVR_cI_c are in the Vega system.

$t - t_0$ (min)	Exposure (s)	Magnitude	Band	Telescope
740.0	720	22.73 ± 0.15	u'	TNG
727.5	240	21.81 ± 0.04	B	TNG
722.0	120	21.37 ± 0.05	V	TNG
2135.0	600	22.85 ± 0.07	V	TNG
716.5	120	21.07 ± 0.05	R_c	TNG
709.5	240	20.44 ± 0.06	I_c	TNG
2197.0	360	21.90 ± 0.15	I_c	TNG

Table A2. TNG data for GRB 050922C. Magnitudes are in the Vega system.

$t - t_0$ (min)	Exposure (s)	Magnitude	Band	Telescope
1700.0	180	22.41 ± 0.03	B	VLT
1686.7	200	22.00 ± 0.02	V	VLT
1692.4	120	21.52 ± 0.04	R_c	VLT

Covino et al. (2005). In the fit we used only data earlier than about 20 min.

GRB 060206 This event was studied by several groups (Woźniak et al. 2006; Monfardini et al. 2006; Stanek et al. 2007; Curran et al. 2007a). We collected optical data from Haislip et al. (2006); Monfardini et al. (2006); Curran et al. (2007a); Stanek et al. (2007) and Oates et al. (2009) in the *Swift*-UVOT v and in the r', R_c, I_c bands, and NIR data from Alatalo et al. (2006) and Terada et al. (2006) in the J, H, K bands. In Table A3 we report Asiago¹⁰ and TNG photometry in the r' and i' bands calibrated by SDSS¹¹ photometry of field stars, which was preliminarily published in Malesani et al. (2006a). The available data come from several different telescopes and in spite of the efforts devoted to cross-calibration by the various authors we had to introduce a 5% systematic error to be added in quadrature. In addition, B and V bands are bluer than Lyman- α at the redshift of this event. As shown, e.g., by Aoki et al. (2009) this spectral range is affected by a dense Lyman- α forest making it difficult to model its absorption. We therefore limited our analysis to data redder than Lyman- α .

¹⁰ <http://www.pd.astro.it/asiago/>

¹¹ <http://skyserver.sdss3.org/dr8/en/>

Table A3. TNG data for GRB 060206. Magnitudes are in the AB system.

$t - t_0$ (min)	Exposure (s)	Magnitude	Band	Telescope
1158.5	2000	19.95 ± 0.06	r'	Asiago
2695.7	3600	21.02 ± 0.06	r'	Asiago
11534.1	3000	23.52 ± 0.35	r'	TNG
1229.2	2700	19.48 ± 0.05	i'	Asiago

Table A4. VLT data for GRB 060814. The host galaxy is likely to dominate these measurements. Magnitudes are in the AB system.

$t - t_0$ (min)	Exposure (s)	Magnitude	Band	Telescope
50.1	900	24.39 ± 0.11	r'	VLT
1469.9	960	24.71 ± 0.20	r'	VLT
89.3	360	24.11 ± 0.22	i'	VLT
1464.4	1440	24.56 ± 0.31	i'	VLT

GRB 060210 Data for this event were published by Stanek et al. (2007), R_c , Curran et al. (2007b), R_c and I_c , and Cenko et al. (2009), R_c, i' and z' bands. Unfortunately, as already pointed out by Kann et al. (2010), there is a calibration offset between I_c data from Curran et al. (2007b) and i data from Cenko et al. (2009). We had therefore to add in quadrature a 5% systematic error.

GRB 060306 No afterglow detection was reported for this event. Upper limits are reported by de Pasquale et al. (2006b) in the *Swift*-UVOT bands and by Nysewander et al. (2006); Chen et al. (2006a) and Lamb et al. (2006) in the NIR. Only a lower limit for A_V could be derived. The redshift for this event was questioned by Jakobsson et al. (2012); Krühler et al. (2012), and a solution at lower redshift is reported by Perley et al. (2013).

GRB 060614 This low-redshift event was widely followed. We collected *Swift*-UVOT $uvw2, uvm2, uvw1, u, b, v$ and wh data from Mangano et al. (2007) and B, V, R_c, I_c, J, K data from Della Valle et al. (2006). These two main datasets show small calibration inconsistencies and we had to introduce a 5% systematic error to be added in quadrature.

GRB 060814 The afterglow was detected in the NIR (Levan et al. 2006a; Cenko et al. 2006a; Levan et al. 2006b), with its emission already contaminated by the relatively bright host galaxy. The same is true for our r' and i' VLT observations calibrated by SDSS photometry of field stars, which were preliminarily discussed in Malesani et al. (2006b) and reported in Table A4. We derived a lower limit on A_V assuming that the afterglow cannot be brighter than these detection, likely dominated by the host galaxy contribution. With reference to Figure 9 in Jakobsson et al. (2012) we have tried to isolate the photometry of object A only.

GRB 060904A No adequately calibrated observations of this afterglow have been published, and the redshift is also not known.

GRB 060908 Data for this event are collected by Cenko et al. (2009) (g', R_c, i' and z' bands) and Covino et al. (2010) (*Swift*-UVOT u, v and wh and B, V, R_c, I_c, J, H and K bands). The total dataset is remarkable although due to the many different telescope/instrument combinations we had to add in quadrature an 8% systematic error, as already discussed in Covino et al. (2010).

GRB 060912A Data for this event are collected from Oates et al. (2009) in the *Swift*-UVOT

uvw2, *uvm2*, *uvw1*, *u*, *b*, *v* and *wh* bands and from Deng et al. (2009) in the R_c band. Lyman- α absorption affecting the bluest *Swift*-UVOT filter was modeled superposing to the power-law SED a Voigt profile with parameters reported in Deng et al. (2009).

GRB 060927 Calibrated data for this event were reported by Ruiz-Velasco et al. (2007) in the i' , R_c , I_c and K bands. The R_c band flux was corrected for Lyman- α absorption with parameters obtained by Ruiz-Velasco et al. (2007).

GRB 061007 Data are collected from Mundell et al. (2007) (R_c band) and Schady et al. (2007) (*Swift*-UVOT *uvw1*, *u*, *b*, *v* and *wh* bands). Cross-calibrations of the datasets required to add in quadrature a 3% systematic error.

GRB 061021 Data are collected from Oates et al. (2009) in the *Swift*-UVOT *uvw2*, *uvm2*, *uvw1*, *u*, *b*, *v* and *wh* bands.

GRB 061121 Data are collected from Oates et al. (2009) in the *Swift*-UVOT *uvw1*, *u*, *b*, *v* and *wh* bands and from Kann et al. (2010) in the V , R_c and I_c bands. We removed the *uvw1* band since it is likely heavily affected by Lyman- α absorption.

GRB 061222A Only K band afterglow detection was reported by Cenko et al. (2006b,c). The available NIR data can not constrain the fit parameters and we derived the extinction by extrapolating the X-ray spectrum.

GRB 070306 Data in the H and K bands are collected from Jaunsen et al. (2008).

GRB 070328 No afterglow detection was reported for this event and the redshift is not known. Upper limits in *Swift*-UVOT bands are reported by Marshall et al. (2007).

GRB 070521 No solid afterglow detection was reported for this event. The available photometry refers to the relatively bright host galaxy. Upper limits from Minezaki et al. (2007) have been used to derive a lower limit on A_V .

GRB 071020 Data are collected from Cenko et al. (2009) in the R_c , i' and z' bands and from Bloom et al. (2007) in the J and H bands. The light curve of this event shows a considerable scatter, and we had to add in quadrature an 11% systematic error.

GRB 071112C Data in the *Swift*-UVOT *uvw1*, *u*, *b*, *v* and *wh* bands were collected from Oates et al. (2007b). NIR J and K bands data were collected from Uehara et al. (2010) and V , R_c and I_c bands were collected from Huang et al. (2012). g' , r' and i' bands observations obtained at Asiago and TNG and calibrated following the SDSS are reported in Table A5.

GRB 071117 The afterglow discovery was reported by Bloom et al. (2007b,c). The redshift was derived by Jakobsson et al. (2007) when the host galaxy was likely already dominating the afterglow light. Data in Table A6, calibrated

Table A5. Asiago and TNG data for GRB 071112C. Magnitudes are in the AB system.

$t - t_0$ (min)	Exposure (s)	Magnitude	Band	Telescope
97.7	600	20.88 ± 0.15	g'	Asiago
119.7	300	20.90 ± 0.17	r'	Asiago
126.7	300	21.01 ± 0.28	i'	Asiago
3274.4	300	24.04 ± 0.09	r'	TNG
32036.9	600	22.36 ± 0.12	i'	TNG
125409.9	600	23.93 ± 0.20	i'	TNG

Table A6. VLT and Gemini-S observations of GRB 071117. Magnitudes are in the Vega system.

$t - t_0$ (min)	Exposure (s)	Magnitude	Band	Telescope
558	300	23.04 ± 0.10	R_c	VLT
574	900	23.02 ± 0.04	R_c	Gemini-S
694	540	23.02 ± 0.05	R_c	VLT
2009	1440	23.53 ± 0.04	R_c	Gemini-S

by standard stars observed with the VLT, supersede those reported in Bloom et al. (2007b,c) and Jakobsson et al. (2007). These data and upper limits from Berger & Gonzalez (2007) do not allow to constrain the rest frame extinction.

GRB 080319B This is the famous “naked eye” burst. Data in the V were collected from Pandey et al. (2009). From Bloom et al. (2009) we used data in r' band and in the B , V , R_c and I_c bands. Finally, data in the *Swift*-UVOT *uvw2*, *uvm2*, *uvw1*, *u*, *b*, *v* and *wh* bands and in the R_c , I_c bands were obtained from Racusin et al. (2008). We however did not consider in the fit the *Swift*-UVOT *uvw2*, *uvm2* and *uvw1* filters for possible Lyman- α contamination. In addition in many cases the reported photometric errors are likely neglecting the absolute calibration error judging from the unrealistic small quoted uncertainties. Therefore we had to add in quadrature a 3% systematic error.

GRB 080319C Data are collected from Cenko et al. (2009) in the R_c , i' and z' bands.

GRB 080413B Data in the g' , r' , i' and z' bands, in the J , H and K_s bands and in the *Swift*-UVOT v band were collected from Filgas et al. (2011a). We added in quadrature a 3% systematic error to compensate for the very low photometric errors of the available data possibly neglecting absolute calibration uncertainties.

GRB 080430 The only reliably calibrated data published so far for this event are in the *Swift*-UVOT *uvw2*, *uvm2*, *uvw1*, *u*, *b*, *v* and *wh* bands from Landsman et al. (2008).

GRB 080602 No afterglow detection has been published for this event. In addition the available XRT data do not allow a meaningful comparison with available optical upper limits as in Malesani et al. (2008a).

Table A7. REM data for GRB080916A. Magnitudes are in the Vega system.

$t - t_0$ (min)	Exposure (s)	Magnitude	Band	Telescope
1.27	50	13.78 ± 0.06	<i>H</i>	REM
2.59	50	14.49 ± 0.11	<i>H</i>	REM
3.92	50	14.12 ± 0.08	<i>H</i>	REM
5.26	50	14.13 ± 0.08	<i>H</i>	REM
6.41	25	14.37 ± 0.14	<i>H</i>	REM
16.25	100	15.14 ± 0.15	<i>H</i>	REM

GRB 080603B Data in the *Swift*-UVOT *uvw1, u, b* and *v* bands were collected from Kuin et al. (2008). Data in the *g', r'* and *i'* bands were collected from Jélinek et al. (2012), and in the *J, H* and *K* bands from Miller et al. (2008). We did not use data bluer than the Lyman- α line at this GRB redshift due to strong flux suppression (see, e.g. Jélinek et al. 2012).

GRB 080605 Data in the *g', r', i'* and *z'* bands and in the *J, H* and *K_s* bands were collected from Zafar et al. (2012).

GRB 080607 Data in the *Swift*-UVOT *v* band were collected from Schady et al. (2008). Data in the *V, R_c, I_c, J, J* and *K_s* bands, and in the *i'* and *z'* bands were collected from Perley et al. (2011). We added in quadrature a 5% systematic error to compensate for cross-calibration problems and intrinsic short-term variability in the data.

GRB 080613B No optical afterglow detection has been reported.

GRB 080721 Data in the *V* and *R_c*, and in the *r'* and *i'* bands were collected from Starling et al. (2009). We did not consider data bluer than Lyman- α .

GRB 080804 Data in the *Swift*-UVOT *u, b, v* and *wh* bands were collected from Kuin et al. (2008b) and data from GCN circulars to define the temporal decay only.

GRB 080916A Data in the *Swift*-UVOT *u, b, wh* bands were collected from Oates et al. (2008); Ziaepour et al. (2008). *H* band observations obtained with REM and calibrated following 2MASS stars in the field are reported in Table A7.

GRB 081007 Data in the *Swift*-UVOT *u, b, v, wh* bands, in the *B, V, R_c, I_c, H* and *K_s* and in the *r'* and *i'* bands were collected from Jin et al. (2013). Due to the large number of detectors/telescopes involved we had to add in quadrature a 7% systematic error to compensate for cross-calibration problems.

GRB 081121 Data in the *Swift*-UVOT *u, b, v* and *wh* bands were collected from Oates et al. (2008b). Data in the *g', r', i', z', J, H* and *K_s* were collected from Loew et al. (2008).

GRB 081203A Data in the *Swift*-UVOT *uvw2, uvw1, u, b, v* and *wh* bands were collected from

Table A8. REM data for GRB081222. *J, H* and *K_s* magnitudes are in the Vega system, *r'* magnitudes in the AB system.

$t - t_0$ (min)	Exposure (s)	Magnitude	Band	Telescope
1.37	50	11.24 ± 0.09	<i>H</i>	REM
2.69	50	12.24 ± 0.10	<i>H</i>	REM
4.02	50	12.95 ± 0.07	<i>H</i>	REM
10.01	30	15.94 ± 0.11	<i>r'</i>	REM
10.67	30	16.00 ± 0.11	<i>r'</i>	REM
11.32	30	16.10 ± 0.12	<i>r'</i>	REM
11.98	30	16.28 ± 0.13	<i>r'</i>	REM
12.61	150	14.57 ± 0.07	<i>H</i>	REM
12.63	30	16.28 ± 0.14	<i>r'</i>	REM
12.29	30	16.30 ± 0.14	<i>r'</i>	REM
13.94	30	16.36 ± 0.15	<i>r'</i>	REM
14.59	30	16.20 ± 0.16	<i>r'</i>	REM
17.27	30	16.51 ± 0.17	<i>r'</i>	REM
17.92	30	16.68 ± 0.19	<i>r'</i>	REM
18.58	30	16.62 ± 0.18	<i>r'</i>	REM
19.23	30	16.73 ± 0.20	<i>r'</i>	REM
19.89	30	16.63 ± 0.18	<i>r'</i>	REM
28.08	150	15.93 ± 0.15	<i>J</i>	REM

de Pasquale et al. (2008) and Kuin et al. (2009). *R_c* data were collected from Fatkhullin et al. (2008). We did not consider data bluer than Lyman- α .

GRB 081221 No afterglow detection has been reported for this event. The upper limit reported by Malesani et al. (2008b) was used to derive a lower limit for A_V .

GRB 081222 Data in the *Swift*-UVOT *u, b, v* and *wh* bands were collected from Breeveld et al. (2008). Data in the *J, H* and *K_s* bands from Updike et al. (2008). REM photometry is reported in Table A8. These data update and substitute those reported in Covino et al. (2008b). NIR data were calibrated with 2MASS stars in the field and optical data with stars reported in the APASS catalogue¹². We did not consider data bluer than Lyman- α . We had to add in quadrature a 7.5% systematic error to compensate the unrealistic low errors reported in some of the available photometry possibly neglecting absolute calibration uncertainties.

GRB 090102 Data in the *Swift*-UVOT *u, b, v* and *wh* bands were collected from Curran et al. (2009). Data in the *g', R_c, i', z', J, H* and *K_s* were collected from Gendre et al. (2010).

GRB 090201 The afterglow detection, likely already substantially contaminated by the host galaxy, was reported by D'Avanzo et al. (2009). Data reported in D'Avanzo et al. (2009) are superseded by those reported in Table A9. Optical data were calibrated by observation of standard star frames and NIR data following the 2MASS catalogue. The redshift for this event is reported in Krühler et al. (2013b).

GRB 090424 Data in the *Swift*-UVOT *u, b, v, wh* bands and in the *R_c* and *I_c* were collected from Jin et al. (2013).

¹² <http://www.aavso.org/apass>

Table A9. VLT data for GRB090201. Magnitudes are in the Vega system.

$t - t_0$ (min)	Exposure (s)	Magnitude	Band	Telescope
434.0	720	24.12 ± 0.08	R_c	VLT
916574	5000	24.40 ± 0.09	R_c	NTT
451.0	480	23.75 ± 0.11	I_c	VLT
554.0	1200	22.05 ± 0.13	J	VLT
580.4	1200	21.31 ± 0.15	H	VLT
608.0	1200	20.19 ± 0.14	K_s	VLT

Data in the g', r', i', z', J, H and K_s were collected from Olivares et al. (2009). Data in the V, I_c, J and K_s bands from Cobb (2009a). Due to the large number of detectors/telescopes involved we had to add in quadrature a 7.5% systematic error to compensate for cross-calibration problems.

GRB 090709A Data in the z', J, H and K_s bands were collected from Cenko et al. (2010). The redshift for this event is reported by Perley et al. (2013). Data show a considerable scatter, and we had to add in quadrature a 9% systematic error.

GRB 090715B Data in the R_c and I_c bands were collected from Haislip et al. (2009), data in the r', i' and z' from Virgili et al. (2013, in preparation).

GRB 090812 Data in the *Swift*-UVOT u and b bands were collected from Schady et al. (2009). Data in the g', r', i', z' and j bands were collected from Updike et al. (2009) and Virgili et al. (2013, in preparation). We did not use data bluer than Lyman- α .

GRB 090926B No reliably calibrated data have been published for this event although in Greiner et al. (2011) a SED analysis was reported. Upper limits from Xu et al. (2009) did not allow to constrain rest frame extinction.

GRB 091018 Data in the *Swift*-UVOT $uvw1, u, b, v, wh$ bands, in the g', r', i', z' bands, and in the J, H and K bands were collected from Wiersema et al. (2012). Due to the large number of detectors/telescopes involved we had to add in quadrature a 2.5% systematic error to compensate for cross-calibration problems.

GRB 091020 Data in the *Swift*-UVOT $uvw1, u, b, v$ and wh bands were collected from Oates et al. (2009b) and Racusin et al. (2009) and in the B, V, R_c and I_c from Kann et al. (2009a,b). We did not use data bluer than Lyman- α .

GRB 091127 Data in the g', r', i', z', J and H bands were collected from Filgas et al. (2011b), data in the I_c band from Vergani et al. (2011), data in the *Swift*-UVOT $uvw1$ and u bands, and in the B, V, R_c and I_c bands from Cobb (2010). Due to the large number of detectors/telescopes involved we had to add in quadrature a 2% systematic error to compensate for cross-calibration problems.

GRB 091208B Data in the *Swift*-UVOT u and b bands were collected from de Pasquale et al. (2009), data in the g', r', i', z', J and H bands were collected from Updike et al. (2009b). We however did not use data bluer than Lyman- α and collected not-properly calibrated data from GCNs to constrain the temporal decay only.

GRB 100615A No detection is reported for this afterglow. Upper limits are discussed in D'Elia & Stratta (2011). Redshift was recently measured by Krühler et al. (2013a).

GRB 100621A Data in the g', r', i', z', J, H and K_s bands were collected from Krühler et al. (2011) and data in the J, H and K_s were collected from Naito et al. (2010). Data from Krühler et al. (2011) are late enough to be considerably affected by the host galaxy brightness, in particular in the bluest available bands. We deal with this uncertainty by adding in quadrature a 7.5% systematic error.

GRB 100728B Data in the *Swift*-UVOT u, b and wh bands were collected from Oates et al. (2010), data in the R_c band from Volnova et al. (2010) and data in the J, H and K_s bands from Olivares et al. (2010).

GRB 110205A Data in the *Swift*-UVOT u, b, v and wh bands, in the g', r', i' and z' bands and in the J, H and K_s bands were collected from Cucchiara et al. (2011). Data in the $U, B, V, R_c, I_c, g', r', i'$ and z' bands from Zheng et al. (2012). Data in the B, V, R_c and I_c bands from Gendre et al. (2012). Data in the g', R_c and I_c bands were collected from Kuroda et al. (2011a,b). Finally, data in the r' band were collected from Urata et al. (2011). To compensate for cross-calibration problems in different datasets we added a 2% systematic error. We did not use data bluer than Lyman- α .

GRB 110503A Data in the *Swift*-UVOT $uvw1, uvm2, uvw2, u, b, v$ and wh bands were collected from Oates et al. (2011) and data in the J and H bands were collected from Morgan & Bloom (2011). To compensate for cross-calibration problems in preliminary datasets we added a 7.5% systematic error. We did not use data bluer than Lyman- α .

This paper has been typeset from a \LaTeX file prepared by the author.

Table A10. Results of the analysis performed in this work for the GRBs in the sample. We report the spectral index and the amount of rest-frame reddening for each applied extinction recipe: MW, LMC and SMC. Spectral slopes and extinctions are computed leaving the spectral slope free or imposing a prior from X-ray data as described in Sect. 2.

Event	t_{\min}, t_{\max} (min)	Ext. curve	No X-ray prior			With X-ray prior		
			β_o	E_{B-V}	χ^2/dof	β_o	E_{B-V}	χ^2/dof
GRB 050318	43, 860	MW	$4.78^{+1.11}_{-1.00}$	$0.27^{+0.20}_{-0.19}$	1.00 (4.00/4)	1.02	0.00	16.25 (65.01/4)
		LMC	$2.23^{+1.14}_{-1.18}$	$0.34^{+0.29}_{-0.18}$	1.00 (4.00/4)	$1.02^{+0.00}_{-0.13}$	$0.57^{+0.17}_{-0.15}$	1.47 (5.86/4)
		SMC	$-2.00^{+3.89}_{-4.90}$	$0.50^{+0.40}_{-0.35}$	1.00 (4.00/4)	$0.89^{+0.13}_{-0.00}$	$0.25^{+0.06}_{-0.06}$	1.25 (5.02/4)
GRB 050401	29, 1400	MW	0.70	0.00	2.16 (12.96/6)	+0.48	0.03	2.41 (14.43/6)
		LMC	-0.41	0.20	1.84 (11.04/6)	+0.19	0.11	2.12 (12.71/6)
		SMC	$-0.42^{+0.65}_{-0.73}$	$0.16^{+0.10}_{-0.09}$	1.43 (8.59/6)	$+0.19^{+0.29}_{-0.00}$	$0.07^{+0.02}_{-0.04}$	1.64 (9.85/6)
GRB 050416A	43, 10000	MW	$0.37^{+0.78}_{-1.03}$	$0.34^{+0.35}_{-0.27}$	0.84 (20.17/24)	$0.48^{+0.24}_{-0.01}$	$0.30^{+0.04}_{-0.12}$	0.84 (20.20/24)
		LMC	$0.87^{+0.39}_{-0.47}$	$0.14^{+0.13}_{-0.10}$	0.78 (18.73/24)	$0.72^{+0.00}_{-0.25}$	$0.18^{+0.09}_{-0.03}$	0.79 (18.98/24)
		SMC	$1.04^{+0.25}_{-0.33}$	$0.08^{+0.08}_{-0.04}$	0.78 (18.60/24)	$0.72^{+0.00}_{-0.17}$	$0.16^{+0.05}_{-0.03}$	0.86 (20.73/24)
GRB 050525A	2.9, 7.8	MW	1.48	0.00	2.16 (38.92/18)	0.73	0.17	3.02 (54.36/18)
		LMC	0.73	0.10	1.81 (32.63/18)	0.73	0.10	1.82 (32.84/18)
		SMC	$0.27^{+0.48}_{-0.52}$	$0.12^{+0.05}_{-0.04}$	1.42 (25.63/18)	$0.45^{+0.28}_{-0.00}$	$0.10^{+0.00}_{-0.03}$	1.45 (26.06/18)
GRB 050802	86, 2900	MW	$1.78^{+0.31}_{-0.42}$	$< 0.16(0.01)$	1.71 (10.47/6)	0.43	0.22	4.70 (28.23/6)
		LMC	$0.79^{+1.08}_{-1.24}$	$< 0.55(0.13)$	1.51 (9.05/6)	$0.43^{+0.00}_{-0.11}$	$0.17^{+0.05}_{-0.03}$	1.53 (9.21/6)
		SMC	$0.34^{+1.10}_{-1.42}$	$< 0.43(0.13)$	1.31 (7.85/6)	$0.34^{+0.09}_{-0.02}$	$0.13^{+0.03}_{-0.03}$	1.31 (7.85/6)
GRB 050922C	3.9, 16	MW	$1.21^{+0.25}_{-0.63}$	$< 0.09(0.01)$	1.20 (19.22/16)	$0.81^{+0.00}_{-0.13}$	$0.05^{+0.02}_{-0.01}$	1.25 (19.92/16)
		LMC	$0.79^{+0.68}_{-2.02}$	$< 0.22(0.04)$	1.20 (19.21/16)	$0.78^{+0.03}_{-0.10}$	$0.04^{+0.01}_{-0.01}$	1.20 (19.21/16)
		SMC	$-0.30^{+1.47}_{-4.74}$	$< 0.56(0.10)$	1.20 (19.21/16)	$0.68^{+0.13}_{-0.00}$	$0.03^{+0.01}_{-0.01}$	1.20 (19.21/16)
GRB 060206	72, 330	MW	$0.85^{+0.07}_{-0.33}$	$< 0.13(0.00)$	1.76 (8.79/5)	$0.85^{+0.07}_{-0.33}$	$< 0.13(0.00)$	1.76 (8.79/5)
		LMC	$0.02^{+0.64}_{-0.60}$	$0.11^{+0.08}_{-0.08}$	1.14 (5.72/5)	$0.27^{+0.50}_{-0.00}$	$0.08^{+0.01}_{-0.07}$	1.20 (6.01/5)
		SMC	$0.46^{+0.41}_{-0.39}$	$< 0.09(0.04)$	1.39 (6.93/5)	$0.46^{+0.41}_{-0.39}$	$< 0.06(0.04)$	1.39 (6.93/5)
GRB 060210	8.6, 43	MW	$4.47^{+0.28}_{-1.68}$	$< 1.00(0.00)$	1.06 (22.29/21)	$1.13^{+0.00}_{-0.10}$	$0.60^{+0.10}_{-0.07}$	1.24 (26.14/21)
		LMC	$4.47^{+0.28}_{-4.86}$	$< 0.96(0.00)$	1.06 (22.29/21)	$1.13^{+0.00}_{-0.10}$	$0.28^{+0.05}_{-0.04}$	1.13 (23.77/21)
		SMC	$4.47^{+0.28}_{-9.51}$	$< 0.71(0.00)$	1.06 (22.29/21)	$1.13^{+0.00}_{-0.10}$	$0.20^{+0.03}_{-0.02}$	1.10 (23.01/21)
GRB 060306	96	MW				0.86	> 2.8	
		LMC				0.86	> 2.7	
		SMC				0.86	> 3.0	
GRB 060614	2300, 5300	MW	0.07	0.33	2.04 (18.40/9)	0.35	0.24	2.38 (21.43/9)
		LMC	$0.03^{+0.23}_{-0.26}$	$0.31^{+0.07}_{-0.07}$	1.39 (12.48/9)	0.35	0.22	1.84 (16.90/9)
		SMC	$0.18^{+0.20}_{-0.23}$	$0.26^{+0.07}_{-0.06}$	1.36 (12.28/9)	$0.35^{+0.09}_{-0.00}$	$0.22^{+0.02}_{-0.02}$	1.52 (13.66/9)
GRB 060814	50	MW				0.56	> 0.4	
		LMC				0.56	> 0.4	
		SMC				0.56	> 0.4	
GRB 060904A		MW						
		LMC						
		SMC						
GRB 060908	8.6, 290	MW	$0.38^{+0.06}_{-0.07}$	$< 0.01(0.00)$	0.99 (87.80/89)	$0.56^{+0.02}_{-0.00}$	$< 0.01(0.00)$	1.14 (101.60/89)
		LMC	$0.38^{+0.06}_{-0.17}$	$< 0.04(0.00)$	0.99 (87.80/89)	$0.56^{+0.02}_{-0.00}$	$< 0.01(0.00)$	1.14 (101.60/89)
		SMC	$0.22^{+0.19}_{-0.21}$	$< 0.07(0.02)$	0.97 (86.50/89)	$0.56^{+0.02}_{-0.00}$	$< 0.01(0.00)$	1.14 (101.60/89)
GRB 060912A	8.6, 290	MW	$1.07^{+0.15}_{-0.64}$	$< 0.41(0.00)$	0.87 (16.44/19)	$0.90^{+0.00}_{-0.44}$	$< 0.22(0.03)$	0.89 (16.90/19)
		LMC	$0.25^{+0.97}_{-1.60}$	$< 0.53(0.13)$	0.83 (15.77/19)	$0.46^{+0.44}_{-0.00}$	$< 0.16(0.10)$	0.83 (15.82/19)
		SMC	$-0.08^{+1.23}_{-1.42}$	$< 0.41(0.14)$	0.77 (14.71/19)	$0.46^{+0.44}_{-0.00}$	$0.07^{+0.02}_{-0.06}$	0.79 (15.07/19)
GRB 060927	14, 4500	MW	$0.75^{+0.41}_{-0.54}$	$< 0.17(0.00)$	1.75 (6.98/4)	$0.75^{+0.41}_{-0.04}$	$< 0.10(0.00)$	1.75 (6.98/4)
		LMC	$0.75^{+0.41}_{-1.45}$	$< 0.41(0.00)$	1.75 (6.98/4)	$0.75^{+0.41}_{-0.04}$	$< 0.08(0.00)$	1.75 (6.98/4)
		SMC	$0.75^{+0.41}_{-2.35}$	$< 0.47(0.00)$	1.75 (6.98/4)	$0.75^{+0.41}_{-0.04}$	$< 0.06(0.00)$	1.75 (6.98/4)

Table A10 – *continued*

GRB 061007	7.2, 22	MW	2.36	0.13	1.80 (117.23/65)	1.10	0.37	11.05 (718.29/65)
		LMC	$0.87^{+0.27}_{-0.24}$	$0.24^{+0.03}_{-0.04}$	1.19 (77.40/65)	$0.97^{+0.13}_{-0.02}$	$0.23^{+0.01}_{-0.01}$	1.20 (77.76/65)
		SMC	$-0.30^{+0.40}_{-0.42}$	$0.24^{+0.03}_{-0.03}$	1.18 (76.94/65)	0.95	0.14	1.44 (93.84/65)
GRB 061021	58, 360	MW	$0.40^{+0.09}_{-0.28}$	< 0.14(0.00)	0.45 (7.65/17)	$0.45^{+0.09}_{-0.00}$	< 0.04(0.00)	0.47 (7.93/17)
		LMC	$-0.31^{+0.80}_{-1.03}$	< 0.35(0.11)	0.38 (6.52/17)	$0.45^{+0.09}_{-0.00}$	< 0.02(0.00)	0.47 (7.93/17)
		SMC	$0.04^{+0.45}_{-0.60}$	< 0.15(0.04)	0.40 (6.88/17)	$0.45^{+0.09}_{-0.00}$	< 0.02(0.00)	0.47 (7.93/17)
GRB 061121	50, 1300	MW	$0.72^{+0.21}_{-0.20}$	< 0.10(0.00)	0.96 (15.34/16)	$0.47^{+0.00}_{-0.12}$	< 0.13(0.01)	1.11 (17.75/16)
		LMC	$-0.38^{+1.24}_{-2.52}$	< 0.69(0.18)	0.93 (14.82/16)	$0.35^{+0.12}_{-0.00}$	$0.06^{+0.03}_{-0.05}$	0.94 (15.06/16)
		SMC	$-1.15^{+1.21}_{-1.41}$	$0.19^{+0.14}_{-0.13}$	0.72 (11.55/16)	$0.35^{+0.12}_{-0.00}$	$0.04^{+0.02}_{-0.03}$	0.87 (13.96/16)
GRB 061222A	126	MW				$0.95^{+0.07}_{-0.06}$	$0.90^{+0.30}_{-0.30}$	
		LMC				$0.95^{+0.07}_{-0.06}$	$0.90^{+0.40}_{-0.30}$	
		SMC				$0.95^{+0.07}_{-0.06}$	$1.00^{+0.40}_{-0.30}$	
GRB 070306	1400, 5800	MW				$0.39^{+0.13}_{-0.00}$	$1.95^{+0.52}_{-0.44}$	∞ (1.40/0)
		LMC				$0.39^{+0.13}_{-0.00}$	$1.85^{+0.50}_{-0.46}$	∞ (1.40/0)
		SMC				$0.39^{+0.13}_{-0.00}$	$2.02^{+0.52}_{-0.51}$	∞ (1.40/0)
GRB 070328		MW						
		LMC						
		SMC						
GRB 070521	90	MW				0.40	> 0.8	
		LMC				0.40	> 0.7	
		SMC				0.40	> 0.8	
GRB 071020	72, 220	MW	$0.58^{+0.28}_{-1.05}$	< 0.26(0.00)	1.40 (20.97/15)	$0.75^{+0.20}_{-0.00}$	< 0.04(0.00)	1.44 (21.54/15)
		LMC	$0.58^{+0.28}_{-1.38}$	< 0.36(0.00)	1.40 (20.97/15)	$0.75^{+0.20}_{-0.00}$	< 0.05(0.00)	1.44 (21.54/15)
		SMC	$0.58^{+0.28}_{-1.71}$	< 0.40(0.00)	1.40 (20.97/15)	$0.75^{+0.20}_{-0.00}$	< 0.05(0.00)	1.44 (21.54/15)
GRB 071112C	5.8, 22	MW	$0.48^{+0.19}_{-0.40}$	< 0.17(0.00)	1.03 (33.86/33)	$0.49^{+0.01}_{-0.40}$	< 0.17(0.00)	1.03 (33.86/33)
		LMC	$0.48^{+0.19}_{-0.44}$	< 0.13(0.00)	1.03 (33.86/33)	$0.49^{+0.01}_{-0.44}$	< 0.13(0.00)	1.03 (33.86/33)
		SMC	$0.48^{+0.19}_{-0.37}$	< 0.10(0.00)	1.03 (33.86/33)	$0.49^{+0.01}_{-0.37}$	< 0.10(0.00)	1.03 (33.86/33)
GRB 071117		MW						
		LMC						
		SMC						
GRB 080319B	72, 860	MW	$0.39^{+0.02}_{-0.02}$	< 0.01(0.00)	1.12 (110.87/99)	$0.38^{+0.00}_{-0.02}$	< 0.01(0.00)	1.12 (110.98/99)
		LMC	$0.38^{+0.02}_{-0.04}$	< 0.02(0.00)	1.12 (110.87/99)	$0.38^{+0.00}_{-0.04}$	< 0.02(0.00)	1.12 (110.98/99)
		SMC	$0.22^{+0.15}_{-0.15}$	$0.03^{+0.02}_{-0.02}$	1.09 (108.32/99)	$0.26^{+0.11}_{-0.00}$	< 0.02(0.02)	1.10 (108.46/99)
GRB 080319C	18, 36	MW	$1.61^{+0.62}_{-0.68}$	$0.06^{+0.05}_{-0.05}$	0.89 (1.79/2)	0.75	0.13	2.52 (5.04/2)
		LMC	$1.37^{+0.86}_{-0.88}$	$0.11^{+0.09}_{-0.09}$	0.89 (1.79/2)	$0.75^{+0.00}_{-0.49}$	$0.17^{+0.05}_{-0.02}$	1.41 (2.82/2)
		SMC	$0.48^{+1.66}_{-1.64}$	$0.26^{+0.23}_{-0.23}$	0.89 (1.79/2)	$0.48^{+0.27}_{-0.24}$	$0.26^{+0.06}_{-0.07}$	0.89 (1.79/2)
GRB 080413B	19, 100	MW	$0.23^{+0.04}_{-0.05}$	$0.02^{+0.01}_{-0.01}$	0.92 (140.08/153)	$0.40^{+0.01}_{-0.00}$	< 0.01(0.00)	1.09 (166.49/153)
		LMC	$0.19^{+0.07}_{-0.07}$	$0.03^{+0.01}_{-0.01}$	0.91 (139.90/153)	$0.40^{+0.01}_{-0.00}$	< 0.01(0.00)	1.09 (166.49/153)
		SMC	$0.13^{+0.08}_{-0.08}$	$0.04^{+0.01}_{-0.01}$	0.92 (140.28/153)	$0.40^{+0.01}_{-0.00}$	< 0.01(0.00)	1.09 (166.49/153)
GRB 080430	1.4, 180	MW	$0.69^{+0.60}_{-0.55}$	$0.12^{+0.12}_{-0.11}$	1.30 (5.19/4)	$0.50^{+0.12}_{-0.06}$	$0.14^{+0.04}_{-0.05}$	1.68 (6.72/4)
		LMC	$0.50^{+0.95}_{-1.27}$	< 0.28(0.10)	1.65 (6.62/4)	$0.49^{+0.13}_{-0.00}$	$0.10^{+0.02}_{-0.04}$	1.65 (6.62/4)
		SMC	$1.12^{+0.37}_{-1.00}$	< 0.15(0.02)	1.86 (7.45/4)	0.62	0.06	1.98 (7.94/4)
GRB 080602		MW						
		LMC						
		SMC						
GRB 080603B	160, 720	MW	$0.52^{+0.25}_{-0.30}$	< 0.06(0.00)	0.41 (1.22/3)	$0.54^{+0.09}_{-0.33}$	< 0.06(0.00)	0.41 (1.23/3)
		LMC	$0.52^{+0.25}_{-0.67}$	< 0.35(0.00)	0.41 (1.22/3)	$0.54^{+0.09}_{-0.38}$	< 0.20(0.00)	0.41 (1.23/3)
		SMC	$0.22^{+0.65}_{-0.74}$	< 0.16(0.05)	0.26 (0.77/3)	$0.19^{+0.44}_{-0.03}$	< 0.06(0.05)	0.26 (0.77/3)
GRB 080605	72, 220	MW	1.57	0.00	3.42 (30.81/9)	0.97	0.12	2.86 (88.34/153)
		LMC	0.98	0.12	2.52 (22.69/9)	0.97	0.12	2.52 (22.69/9)
		SMC	$0.65^{+0.24}_{-0.22}$	$0.16^{+0.04}_{-0.04}$	0.28 (2.49/9)	$0.74^{+0.20}_{-0.04}$	$0.14^{+0.01}_{-0.03}$	0.30 (2.73/9)

Table A10 – continued

GRB 080607	13, 22	MW	$1.73^{+0.27}_{-0.29}$	$0.30^{+0.09}_{-0.07}$	0.87 (7.81/9)	$1.19^{+0.00}_{-0.11}$	$0.43^{+0.03}_{-0.02}$	1.46 (13.14/9)
		LMC	1.28	0.31	4.50 (40.49/9)	1.19	0.33	4.50 (40.53/9)
		SMC	2.94	0.00	5.82 (52.37/9)	1.19	0.25	11.96 (107.67/9)
GRB 080613B		MW						
		LMC						
		SMC						
GRB 080721	580, 58000	MW	$1.34^{+1.09}_{-0.99}$	$< 0.43(0.14)$	0.43 (3.90/9)	$0.96^{+0.00}_{-0.10}$	$< 0.40(0.11)$	0.46 (4.16/9)
		LMC	$-0.23^{+1.57}_{-1.31}$	$< 0.60(0.21)$	0.42 (3.74/9)	$0.86^{+0.10}_{-0.09}$	$< 0.26(0.07)$	0.52 (4.65/9)
		SMC	$-4.13^{+5.13}_{-7.30}$	$< 1.05(0.42)$	0.39 (3.48/9)	$0.86^{+0.10}_{-0.00}$	$< 0.12(0.01)$	0.57 (5.10/9)
GRB 080804	5.8, 72	MW	$0.59^{+2.30}_{-1.06}$	$< 0.53(0.09)$	0.49 (1.97/4)	$0.55^{+0.04}_{-0.19}$	$0.09^{+0.08}_{-0.05}$	0.49 (1.97/4)
		LMC	$-1.74^{+3.39}_{-10.08}$	$< 1.51(0.25)$	0.49 (1.97/4)	$0.36^{+0.23}_{-0.01}$	$0.08^{+0.04}_{-0.05}$	0.51 (2.03/4)
		SMC	$-8.45^{+10.10}_{-18.18}$	$< 1.76(0.59)$	0.49 (1.97/4)	$0.37^{+0.22}_{-0.02}$	$0.06^{+0.03}_{-0.04}$	0.52 (2.07/4)
GRB 080916A	5, 290	MW	$1.47^{+0.09}_{-0.34}$	$< 0.22(0.00)$	1.06 (7.44/7)	$1.20^{+0.00}_{-0.26}$	$0.07^{+0.08}_{-0.02}$	1.30 (9.07/7)
		LMC	$1.47^{+0.09}_{-0.43}$	$< 0.26(0.00)$	1.06 (7.44/7)	$1.20^{+0.00}_{-0.31}$	$0.07^{+0.09}_{-0.02}$	1.24 (8.65/7)
		SMC	$1.47^{+0.09}_{-0.43}$	$< 0.26(0.00)$	1.06 (7.44/7)	$1.20^{+0.00}_{-0.31}$	$0.07^{+0.09}_{-0.02}$	1.24 (8.67/7)
GRB 081007	10, 120	MW	$0.36^{+0.28}_{-0.33}$	$0.13^{+0.09}_{-0.07}$	0.96 (33.38/37)	$0.86^{+0.06}_{-0.00}$	$< 0.04(0.01)$	1.13 (41.97/37)
		LMC	$0.31^{+0.37}_{-0.38}$	$0.14^{+0.10}_{-0.09}$	0.99 (36.68/37)	$0.86^{+0.07}_{-0.00}$	$< 0.04(0.01)$	1.13 (41.97/37)
		SMC	$0.43^{+0.33}_{-0.38}$	$0.11^{+0.09}_{-0.08}$	1.04 (38.49/37)	$0.86^{+0.07}_{-0.00}$	$< 0.04(0.00)$	1.14 (42.15/37)
GRB 081121	43, 430	MW	$-0.13^{+0.25}_{-0.28}$	$0.10^{+0.03}_{-0.03}$	0.65 (3.93/6)	$0.37^{+0.13}_{-0.00}$	$0.08^{+0.01}_{-0.02}$	0.95 (5.71/6)
		LMC	$-0.38^{+0.50}_{-0.43}$	$0.15^{+0.05}_{-0.05}$	0.29 (1.74/6)	$0.37^{+0.11}_{-0.00}$	$0.07^{+0.01}_{-0.01}$	1.43 (8.55/6)
		SMC	$-0.31^{+0.43}_{-0.41}$	$0.11^{+0.03}_{-0.03}$	0.53 (3.18/6)	$0.37^{+0.12}_{-0.00}$	$0.06^{+0.01}_{-0.01}$	1.48 (8.87/6)
GRB 081203A	140, 7200	MW	$0.68^{+0.95}_{-1.31}$	$0.17^{+0.07}_{-0.11}$	0.75 (5.27/7)	$0.66^{+0.11}_{-0.08}$	$0.17^{+0.03}_{-0.03}$	0.75 (5.27/7)
		LMC	$-1.45^{+2.30}_{-2.23}$	$0.29^{+0.16}_{-0.15}$	0.74 (5.15/7)	$0.57^{+0.02}_{-0.17}$	$0.15^{+0.02}_{-0.03}$	0.92 (6.42/7)
		SMC	$-5.92^{+4.51}_{-4.18}$	$0.49^{+0.24}_{-0.25}$	0.74 (5.15/7)	$0.67^{+0.12}_{-0.07}$	$0.12^{+0.02}_{-0.02}$	1.16 (8.14/7)
GRB 081221	190	MW				0.89	> 0.5	
		LMC				0.89	> 0.5	
		SMC				0.89	> 0.5	
GRB 081222	1.2, 43	MW	-0.45	0.02	1.45 (27.54/19)	0.48	$< 0.03(0.02)$	1.45 (27.54/19)
		LMC	$-0.31^{+0.70}_{-0.71}$	$0.15^{+0.12}_{-0.12}$	1.30 (24.68/19)	$0.47^{+0.12}_{-0.00}$	$< 0.03(0.01)$	1.43 (27.19/19)
		SMC	$-0.01^{+0.52}_{-0.54}$	$< 0.19(0.07)$	1.33 (25.19/19)	$0.47^{+0.12}_{-0.00}$	$< 0.02(0.01)$	1.42 (27.03/19)
GRB 090102	4.3, 29	MW	$0.95^{+0.14}_{-0.35}$	$< 0.20(0.00)$	1.06 (6.33/6)	$0.36^{+0.14}_{-0.00}$	$0.14^{+0.06}_{-0.03}$	1.71 (10.27/6)
		LMC	$-0.16^{+1.00}_{-1.00}$	$0.21^{+0.21}_{-0.19}$	0.67 (4.00/6)	$0.22^{+0.14}_{-0.00}$	$0.14^{+0.02}_{-0.05}$	0.71 (4.27/6)
		SMC	$0.27^{+0.54}_{-0.59}$	$0.11^{+0.10}_{-0.09}$	0.54 (3.23/6)	$0.27^{+0.09}_{-0.05}$	$0.11^{+0.03}_{-0.03}$	0.54 (3.23/6)
GRB 090201	434	MW				0.49	> 0.4	
		LMC				0.49	> 0.4	
		SMC				0.49	> 0.4	
GRB 090424	120, 4300	MW	$1.35^{+0.25}_{-0.27}$	$0.09^{+0.09}_{-0.08}$	0.85 (27.24/32)	$0.55^{+0.00}_{-0.06}$	$0.35^{+0.02}_{-0.01}$	1.31 (41.81/32)
		LMC	$1.32^{+0.29}_{-0.21}$	$0.09^{+0.06}_{-0.05}$	0.75 (23.97/32)	0.55	0.31	1.50 (47.97/32)
		SMC	$1.41^{+0.20}_{-0.15}$	$0.06^{+0.04}_{-0.04}$	0.74 (23.80/32)	0.55	0.31	2.15 (68.70/32)
GRB 090709A	1.4, 14	MW	$-0.03^{+3.20}_{-7.64}$	< 5.88	1.84 (9.18/5)	$0.35^{+0.09}_{-0.05}$	$0.83^{+0.16}_{-0.16}$	1.84 (9.19/5)
		LMC	$0.24^{+2.93}_{-7.48}$	< 5.02	1.84 (9.19/5)	$0.44^{+0.00}_{-0.14}$	$0.75^{+0.18}_{-0.11}$	1.84 (9.20/5)
		SMC	1.52	0.45	1.87 (9.36/5)	0.44	0.77	1.90 (9.49/5)
GRB 090715B	8.6, 430	MW	$1.40^{+0.12}_{-0.12}$	$0.18^{+0.07}_{-0.08}$	0.67 (31.94/48)	0.63	0.00	2.24 (107.63/48)
		LMC	$0.11^{+0.38}_{-0.44}$	$0.17^{+0.07}_{-0.06}$	0.66 (31.84/48)	$0.45^{+0.00}_{-0.18}$	$0.11^{+0.01}_{-0.03}$	0.69 (33.20/48)
		SMC	$-1.09^{+0.85}_{-0.91}$	$0.18^{+0.08}_{-0.07}$	0.66 (31.78/48)	$0.45^{+0.00}_{-0.18}$	$0.06^{+0.01}_{-0.02}$	0.79 (38.07/48)
GRB 090812	1.4, 290	MW	$1.24^{+0.26}_{-0.31}$	$< 0.16(0.03)$	1.52 (12.15/8)	0.52	0.16	2.65 (21.20/8)
		LMC	$0.54^{+0.82}_{-0.89}$	$< 0.33(0.12)$	1.31 (10.51/8)	$0.51^{+0.01}_{-0.12}$	$0.12^{+0.04}_{-0.03}$	1.31 (10.52/8)
		SMC	$0.58^{+0.85}_{-1.01}$	$< 0.24(0.08)$	1.38 (11.08/8)	$0.52^{+0.00}_{-0.13}$	$0.08^{+0.03}_{-0.02}$	1.39 (11.09/8)
GRB 090926B		MW						
		LMC						
		SMC						

Table A10 – *continued*

GRB 091018	86, 230	MW	$0.57^{+0.01}_{-0.01}$	$< 0.01(0.00)$	1.15 (93.54/81)	$0.57^{+0.01}_{-0.02}$	$< 0.01(0.00)$	1.16 (93.64/81)
		LMC	$0.57^{+0.01}_{-0.01}$	$< 0.01(0.00)$	1.15 (93.51/81)	$0.57^{+0.01}_{-0.02}$	$< 0.01(0.00)$	1.16 (93.64/81)
		SMC	$0.57^{+0.01}_{-0.06}$	$< 0.02(0.00)$	1.15 (93.51/81)	$0.57^{+0.01}_{-0.06}$	$< 0.02(0.00)$	1.16 (93.64/81)
GRB 091020	12, 720	MW	$2.02^{+0.15}_{-0.16}$	$0.10^{+0.02}_{-0.03}$	1.40 (23.79/17)	0.66	0.29	13.99 (237.76/17)
		LMC	$0.23^{+0.65}_{-0.64}$	$0.35^{+0.10}_{-0.10}$	1.39 (23.61/17)	$0.55^{+0.11}_{-0.00}$	$0.30^{+0.01}_{-0.03}$	1.42 (24.12/17)
		SMC	2.38	0.00	2.70 (45.98/17)	0.66	0.18	4.45 (75.62/17)
GRB 091127	86, 240	MW	$0.23^{+0.02}_{-0.02}$	$0.04^{+0.01}_{-0.01}$	0.93 (367.11/396)	$0.22^{+0.02}_{-0.01}$	$0.04^{+0.01}_{-0.01}$	0.93 (367.23/396)
		LMC	$0.23^{+0.03}_{-0.03}$	$0.04^{+0.01}_{-0.01}$	0.95 (374.56/396)	$0.22^{+0.04}_{-0.02}$	$0.04^{+0.01}_{-0.01}$	0.95 (375.96/396)
		SMC	$0.28^{+0.03}_{-0.02}$	$0.02^{+0.01}_{-0.01}$	0.98 (387.70/396)	$0.29^{+0.00}_{-0.04}$	$0.02^{+0.01}_{-0.01}$	0.98 (387.95/396)
GRB 091208B	580, 1200	MW	$1.24^{+0.53}_{-0.64}$	$< 0.19(0.07)$	1.08 (6.51/6)	$1.07^{+0.00}_{-0.21}$	$0.09^{+0.07}_{-0.03}$	1.11 (6.66/6)
		LMC	$1.08^{+0.68}_{-0.88}$	$< 0.29(0.10)$	1.08 (6.48/6)	$1.07^{+0.00}_{-0.21}$	$0.10^{+0.08}_{-0.03}$	1.08 (6.48/6)
		SMC	$0.94^{+0.83}_{-1.19}$	$< 0.43(0.14)$	1.09 (6.54/6)	$0.94^{+0.13}_{-0.08}$	$0.14^{+0.06}_{-0.07}$	1.09 (6.54/6)
GRB 100615A	24	MW				0.76	> 2.8	
		LMC				0.76	> 2.8	
		SMC				0.76	> 3.2	
GRB 100621A	100, 140	MW	$1.07^{+0.70}_{-0.71}$	$1.16^{+0.26}_{-0.26}$	1.77 (7.08/4)	$1.02^{+0.01}_{-0.12}$	$1.17^{+0.12}_{-0.04}$	1.77 (7.09/4)
		LMC	$1.19^{+0.64}_{-0.65}$	$1.04^{+0.22}_{-0.21}$	1.84 (7.37/4)	$1.03^{+0.00}_{-0.25}$	$1.10^{+0.11}_{-0.03}$	1.88 (7.52/4)
		SMC	1.80	0.87	2.52 (10.09/4)	1.03	1.16	3.49 (13.94/4)
GRB 100728B	2.2, 140	MW	$0.45^{+0.50}_{-0.48}$	$< 0.23(0.08)$	0.45 (2.70/6)	$0.47^{+0.28}_{-0.07}$	$< 0.14(0.07)$	0.45 (2.70/6)
		LMC	$0.29^{+0.66}_{-0.81}$	$< 0.35(0.10)$	0.45 (2.68/6)	$0.40^{+0.35}_{-0.00}$	$< 0.14(0.08)$	0.46 (2.74/6)
		SMC	$0.70^{+0.31}_{-0.46}$	$< 0.17(0.02)$	0.60 (3.58/6)	$0.70^{+0.05}_{-0.30}$	$< 0.11(0.02)$	0.60 (3.58/6)
GRB 110205A	360, 580	MW	1.23	0.00	1.72 (139.47/81)	0.72	0.12	9.00 (729.07/81)
		LMC	$0.55^{+0.10}_{-0.12}$	$0.11^{+0.02}_{-0.01}$	1.18 (95.39/81)	$0.55^{+0.14}_{-0.01}$	$0.11^{+0.01}_{-0.02}$	1.18 (95.40/81)
		SMC	0.78	0.04	1.28 (104.01/81)	0.72	0.05	1.29 (104.57/81)
GRB 110503A	4.3, 720	MW	$1.24^{+0.40}_{-0.45}$	$< 0.23(0.02)$	1.27 (2.55/2)	0.49	0.17	4.64 (9.27/2)
		LMC	$1.29^{+0.36}_{-0.87}$	$< 0.24(0.00)$	1.31 (2.63/2)	$0.49^{+0.00}_{-0.10}$	$0.10^{+0.07}_{-0.05}$	2.21 (4.42/2)
		SMC	$1.28^{+0.36}_{-0.74}$	$< 0.14(0.00)$	1.31 (2.63/2)	0.49	0.06	2.45 (4.90/2)